Journal of Medicinal Chemistry

Article

pubs.acs.org/jmc

An Extended Pyrrolobenzodiazepine–Polyamide Conjugate with Selectivity for a DNA Sequence Containing the ICB2 Transcription Factor Binding Site

Federico Brucoli,[†,‡] Rachel M. Hawkins,[‡] Colin H. James,[‡] Paul J. M. Jackson,[§] Geoff Wells,[‡] Terence C. Jenkins,[∥] Tom Ellis,[⊥] Minal Kotecha,[⊥] Daniel Hochhauser,[⊥] John A. Hartley,[⊥,#] Philip W. Howard,[#] and David E. Thurston*[,§]

[†]School of Science, University of the West of Scotland, Paisley, Scotland, U.K.

[‡]UCL School of Pharmacy, University College London, 29/39 Brunswick Square, London WC1N 1AX, U.K.

[§]Department of Pharmacy, Institute of Pharmaceutical Sciences, King's College London, Britannia House, 7 Trinity Street, London SE1 1DB, U.K.

[∥]School of Science, University of Greenwich, Chatham Maritime, Kent ME4 4TB, U.K.

[⊥]CRUK Drug-DNA Interactions Research Group, University College London, London WC1E 6BT, U.K.

[#]Spirogen Ltd., QMB Innovation Centre, 42 New Road, London E1 2AX, U.K.

Supporting Information

ABSTRACT: The binding of nuclear factor Y (NF-Y) to inverted CCAAT boxes (ICBs) within the promoter region of DNA topoisomerase IIα results in control of cell differentiation and cell cycle progression. Thus, NF-Y inhibitory small molecules could be employed to inhibit the replication of cancer cells. A library of pyrrolobenzodiazepine (PBD) C8-conjugates consisting of one PBD unit attached to tri-heterocyclic polyamide fragments was designed and synthesized. The DNA-binding affinity and sequence selectivity of each compound were evaluated in DNA thermal denaturation and DNase I footprinting assays, and the ability to inhibit binding of NF-Y to ICB1 and ICB2 was studied using an electrophoretic mobility shift assay (EMSA). **3a** was found to be a potent inhibitor of NF-Y binding, exhibiting a 10-fold selectivity for an ICB2 site compared to an ICB1-containing sequence, and showing low nanomolar cytotoxicity toward human tumor cell lines. Molecular modeling and computational studies have provided details of the covalent attachment process that leads to formation of the PBD–DNA adduct, and have allowed the preference of **3a** for ICB2 to be rationalized.

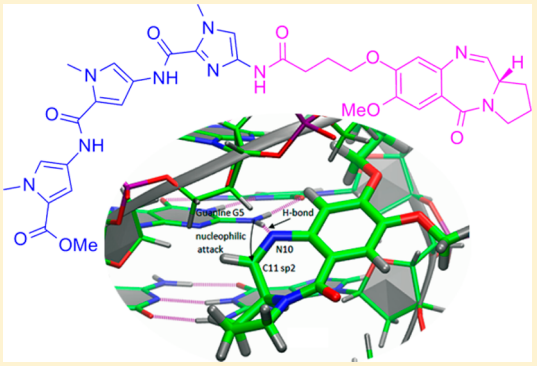

INTRODUCTION

Transcription factor binding sites in disease-related genes are potential therapeutic targets for small molecules. Some low-molecular-weight ligands are known to recognize specific DNA sequences and inhibit transcription factor binding and so could be exploited to modulate transcription and block cellular proliferation.[1−8] Nuclear factor Y (NF-Y) is a ubiquitous CCAAT-binding[9] transcription factor comprising three subunits, NF-YA, NF-YB, and NF-YC, and is involved in cell differentiation and cell cycle progression.[10−12] It has been shown that binding of the heterotrimeric NF-Y to five inverted CCAAT boxes (ICBs) within the promoter region of DNA topoisomerase IIα (Topo IIα) results in control of transcriptional expression at confluence, p53-induced down-regulation, and response to heat-shock-induced up-regulation.[4,13−15] In mammalian cells, Topo IIα represents one of the most important cellular targets for a range of anticancer drugs.[16] High levels of topoisomerase II gene expression correlate with the relative sensitivity of cells to these agents, while low levels confer drug resistance. Binding of NF-Y to ICB2 in confluent cancer cells represses the expression of the Topo IIα gene and contributes to resistance to Topo IIα targeted drugs such as etoposide. For this reason, the regulation of NF-Y/ICB interactions has attracted much interest,[17−19] and it may prove possible to develop sequence-specific DNA-interactive drugs that bind to relevant sequences and block the interaction of transcription factors such as NF-Y, thus modulating the replication of cancer cells.

We have previously reported a library of PBD–poly(*N*-methylpyrrole) conjugates (**1a–f**) consisting of a pyrrolobenzodiazepine (PBD) core attached through the C8-position via a four-carbon linker to between one and six *N*-methylpyrrole units joined through amidic linkages (Figure 1A).[20] These

Received: January 29, 2013

 © XXXX American Chemical Society dx.doi.org/10.1021/jm4001852 | *J. Med. Chem.* XXXX, XXX, XXX–XXX

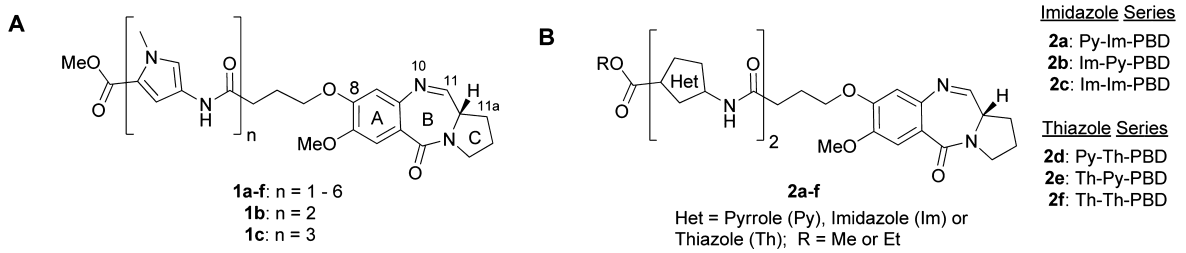

Figure 1. (A) Structures of the C8-linked pyrrolobenzodiazepine–poly(*N*-methylpyrrole) conjugates including **1b** and **1c**. (B) Library of analogues of **1b** containing combinations of imidazole (Im), thiazole (Th), and pyrrole (Py) rings in the C8-polyamide chain (**2a–f**).

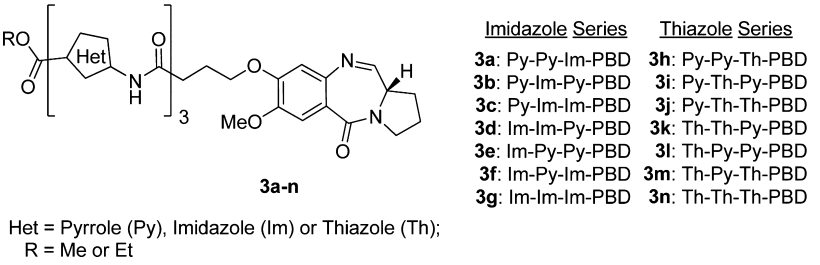

Figure 2. Library of 14 analogues (**3a–n**) of the PBD–heterocycle trimeric polyamide conjugate **1c**.

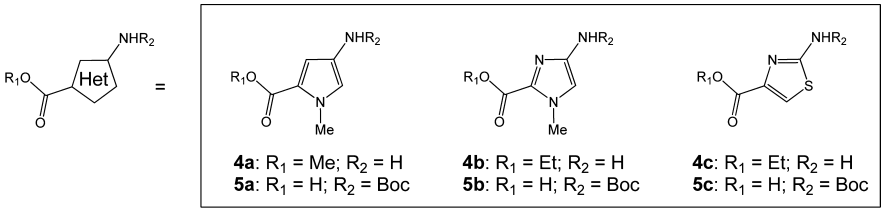

Figure 3. Heterocyclic pyrrole (**4a** and **5a**), imidazole (**4b** and **5b**), and thiazole (**4c** and **5c**) building blocks.

molecules, particularly the dimeric and trimeric conjugates **1b** (known as GWL-78) and **1c**, have generated significant interest in terms of DNA sequence-selectivity and their ability to modulate biological processes such as transcription.[20]

Thermal denaturation studies of DNA binding demonstrated that **1c** produced the greatest ΔT_m shift (21.2 °C) of all members of the series (**1a–f**), indicating that this homologue had the greatest stabilizing effect on duplex DNA. It was found that the ΔT_m for **1c** was 53-fold greater than for the PBD linker unit alone and 5-fold greater than for the tripyrrole unit alone. These data correlated well with the cytotoxicity profiles of the conjugates, with **1c** having the lowest TGI and LC_{50} values across a range of tumor cell lines in the National Cancer Institute (NCI) 60-cell-line panel. Furthermore, Hochhauser and co-workers demonstrated that **1b** could inhibit the binding of NF-Y to the promoter of DNA Topo IIα, and displace NF-Y bound to several CCAAT motifs within the promoters of genes involved in cell cycle progression.[4]

To further investigate the interaction of **1b** with ICB sites, and to attempt to improve both ligand potency and selectivity, we synthesized a library of six analogues of **1b**[2] (**2a–f**) in which the pyrrole residues in the C8-polyamide chain were changed to various combinations of pyrrole (Py), imidazole (Im) and thiazole (Th) rings which are known to affect ligand affinity for DNA[21] (Figure 1B). Thermal denaturation and DNA footprinting assays were employed to assess the DNA-binding affinity and sequence selectivity of these molecules, and their cytotoxicities were determined in the NCI 60-cell-line human tumor panel. The thiazole-containing conjugate **2d** (Py–Th–PBD) emerged as superior to **1b** in terms of overall DNA-binding affinity, selectivity for specific ICB sequences, and growth inhibitory potency.

Following these encouraging results, we decided to extend the series by adding a third heterocycle to lengthen the molecules (Figure 2) and to allow further H-bonding and van der Waals interactions within the host DNA minor groove. In particular, we chose to incorporate Im or Th rings to assess, individually, whether any improvement in affinity or selectivity for individual inverted CCAAT boxes (ICBs) could be achieved. Thus, two new libraries of PBD C8-conjugates were designed containing three heterocyclic rings: the first (**3a–g**) containing Py and/or Im residues; the second (**3h–n**) containing Py and/or Th residues. To obtain SAR data relating to the new C8-heterocyclic polyamide side chains, the DNA-binding affinity and sequence selectivity of each library member were evaluated in DNA thermal denaturation and DNase I footprinting assays, and the ability to inhibit binding of the NF-Y protein to two inverted CCAAT boxes (ICB1 and ICB2) was studied using an electrophoretic mobility shift assay (EMSA). The cytotoxicity of each library member was also evaluated in the NCI 60-cell-line panel. The results allowed ranking of the conjugates from which a lead molecule, **3a**, emerged with significant DNA-binding affinity and sequence selectivity, and the ability to inhibit interaction of the NF-Y transcription factor with ICB2 at the nanomolar level. Crucially, **3a** exhibited a 10-fold selectivity for ICB2 compared to the ICB1 site based on the concentration required to effect inhibition. Although this selectivity between binding sites is modest, these results indicate that it is possible to design small-molecule inhibitors

dx.doi.org/10.1021/jm4001852 | J. Med. Chem. XXXX, XXX, XXX–XXX

Scheme 1. Strategy for the Synthesis of the Heterocyclic Polyamide Components (8a–n) of the PBD Conjugates[a]

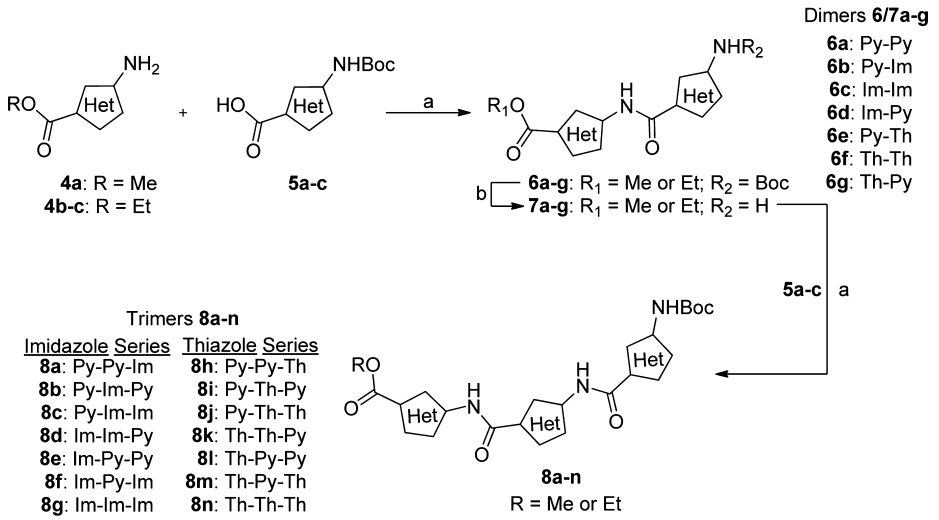

[a](a) EDCI, DMAP, CH_2Cl_2, 18–168 h, 32–99%; (b) 4 M HCl in dioxane, 30 min (imidazole-containing dimers); or CH_2Cl_2/TFA/H_2O, 50:47.5:2.5 v/v, 30 min (thiazole-containing dimers).

Scheme 2. Final Coupling and Deprotection Steps[a]

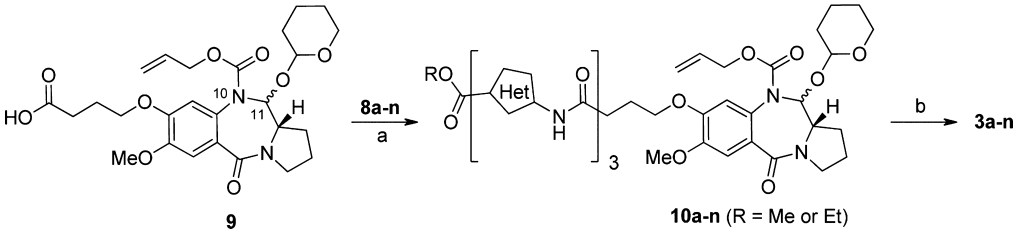

[a](a) EDCI, DMAP, CH_2Cl_2, 24–48 h, 34–95%; (b) $Pd[PPh_3]_4$, pyrrolidine, CH_2Cl_2, 3 h, 10–45%.

that can discriminate between binding sites within a transcription factor family.

RESULTS AND DISCUSSION

Chemistry. The PBD–heterocycle polyamide conjugates (**3a–n**) were prepared in a convergent fashion by joining a PBD capping unit to the appropriate heterocyclic polyamide chain toward the end of the synthetic route. For this reason, preparation of the target molecules was divided into three stages: (1) polyamide assembly, (2) synthesis of the PBD capping unit, and (3) coupling of these two fragments followed by removal of the protective groups. Initially, the heterocyclic amino esters **4a–c** and the Boc-protected heterocyclic acids **5a–c** were prepared as previously reported (Figure 3).[22,23]

Scheme 1 shows the standard solution phase approach used for synthesis of the polyamide components of the target compounds.[20,21] The amino ester heterocycles (**4a–c**) were coupled to the Boc-protected heterocyclic acids (**5a–c**) using EDCI and DMAP to provide the *N*-Boc-protected heterocyclic dimers **6a–g** in sufficient yield and purity to be used directly in the following deprotection step. This was achieved employing different cleaving systems depending on the type of heterocycles present in the dimers. For example, it was found that 4 M HCl in dioxane was a suitable deprotection system for the imidazole/pyrrole-containing dimers, whereas a mixture of CH_2Cl_2/TFA/H_2O (50:47.5:2.5 v/v) was required for the thiazole/pyrrole-containing dimers because of their low solubility in dioxane. The resulting dipeptide amines **7a–g** were subsequently coupled to the Boc-protected acids **5a–c** to furnish the Boc-protected trimers **8a–n**. It is noteworthy that lower yields were observed when coupling a heterocyclic ring to an aminothiazole rather than an aminopyrrole. For example, early attempts to couple the pyrrole acid (**5a**) to the thiazole **4c** resulted in a poor yield (24%) after a reaction time of 60 h. However, the use of further equivalents of the coupling reagents and a longer reaction time (i.e., 168 h) resulted in a significantly higher yield of product (i.e., 70%).

The protected PBD capping unit acid (**9**) was synthesized using a modified version of the Fukuyama approach[20,24] and coupled to the trimeric heterocyclic polyamides **8a–n** to generate the N10-Alloc/C11-*O*-THP-protected conjugates **10a–n** (Scheme 2). Treatment with $Pd[PPh_3]_4$ and pyrrolidine resulted in the concerted removal of both protective groups to provide the target PBD conjugates **3a–n** in their N10-C11 imine forms. With one exception, all final products were obtained in sufficient yields for the biological studies and were purified to ≥95% by mass-directed preparative HPLC prior to evaluation. The Alloc/THP-deprotection of **10j** proved challenging, and only a small quantity of product (**3j**) was obtained in a quantity sufficient only for LCMS identification and not for biological or biophysical evaluation. Compound **1c** (GWL-79)[20] was synthesized from the same PBD intermediate **9** using similar steps and was used as a positive control in the cytotoxicity and thermal denaturation studies (see Supporting Information for analytical data for **1c**). An optical rotation measurement for **1c** (+168°, c = 0.06, $CHCl_3$) demonstrated

dx.doi.org/10.1021/jm4001852 | J. Med. Chem. XXXX, XXX, XXX–XXX

Table 1. NCI Cytotoxicity and DNA Thermal Denaturation Data for the PBD−Heterocycle Conjugates and the Control Molecule 1c

	Compound	Identity	NCI cytotoxicity[a]			Induced ΔT_m (°C)[b] after incubation at 37 ± 0.1 °C for		
			GI_{50} (nm)	TGI (nm)	LC_{50} (μm)	0 h	4 h	18 h
Group 1 (2 × Py)	**3a**	Py−Py−Im−PBD	1.3	24	2.3	19.1	19.8	21.1
	3h	Py−Py−Th−PBD	1.4	30	4.4	16.4	17.4	18.2
	3i	Py−Th−Py−PBD	2.8	50	9.1	18.5	19.9	20.7
	3l	Th−Py−Py−PBD	2.9	28	8.9	16.8	17.7	18.6
	3b	Py−Im−Py−PBD	3.0	20	6.6	15.5	16.0	16.9
	3e	Im−Py−Py−PBD	3.8	37	6.8	16.8	17.6	18.7
	3k	Th−Th−Py−PBD	ND	ND	ND	7.5	8.1	8.4
Group 2 (1 × Py)	**3c**	Py−Im−Im−PBD	3.8	37.0	6.8	14.3	15.0	15.4
	3f	Im−Py−Im−PBD	4.2	141	12.3	14.9	15.7	16.2
	3d	Im−Im−Py−PBD	13.5	27.0	9.5	13.9	14.8	15.2
	3m	Th−Py−Th−PBD	ND	ND	ND	6.4	7.1	7.8
Group 3 (No Py)	**3g**	Im−Im−Im−PBD	87.1	1288	15.4	11.0	11.7	12.0
	3n	Th−Th−Th−PBD	281.8	2042	15.8	10.0	10.7	10.9
Control[c]	**1c**	Py−Py−Py−PBD	15.0	32.0	1.1	17.0	18.7	20.2

[a] GI_{50}, TGI, and LC_{50} values (the concentration causing 50% growth inhibition, total growth inhibition, and 50% lethality, respectively) are the mean values across the NCI 60-cell-line panel. ND = not determined. [b] Induced ΔT_m shift following incubation at 37 ± 0.1 °C for the time shown. The "0 h" values actually reflect ∼30 min of equilibration heating within the instrument used for the T_m assay, which is unavoidable and cannot be circumvented in temperature scan-based assays. Heating was applied at a rate of 1 °C/min in the 50−99 °C temperature range, with optical and temperature data sampling at 100 ms intervals. A separate experiment was carried out using buffer alone, and this baseline was subtracted from each DNA melting curve before data treatment. Experiments were conducted in triplicate. For control CT-DNA alone, T_m = 67.82 ± 0.07 °C (mean from >110 experiments). All ΔT_m values are ±0.1−0.2 °C. For a fixed 1:10 molar ratio of [ligand]/[DNA], DNA concentration was 50 μM (base pairs), and ligand concentration was 5 μM in aqueous sodium phosphate buffer [10 mM sodium phosphate +1 mM EDTA, pH 7.00 ± 0.01]. [c] Thermal denaturation values previously obtained for this PBD conjugate were 17.3 (0 h), 19.6 (4 h), and 21.2 (18 h).[20]

that the biologically active *S*-configuration was retained at the C11a position of the PBD moiety, confirming that racemization had not occurred as a result of the coupling or Alloc/C11-*O*-THP deprotection steps.

Thermal Denaturation Experiments. Thermal denaturation studies using double-stranded calf thymus (CT) DNA were undertaken to investigate the DNA-binding affinity of each PBD−heterocycle conjugate. Melting temperatures (T_m) were determined from optical absorbance versus temperature curves to provide the T_m both for the DNA alone and in the presence of the ligands. The change in T_m (ΔT_m) following incubation of CT-DNA with the conjugates was then calculated from:

$$\Delta T_m = T_{m(DNA-drug)} - T_{m(DNA)}$$

The increase in helix melting temperature for each compound was measured after 0, 4, and 18 h of incubation at 37 °C (Table 1). The data show that all the novel PBD conjugates increased the thermal stability of the duplex DNA significantly. As expected, all compounds showed the characteristic kinetic effect of a PBD upon incubation with DNA, with the induced ΔT_m shifts increasing with time to reach a stable maximal value due to the covalent reaction between the PBD N10-C11 imine moiety and the C2-NH_2 of a guanine base.[25−28] Previous T_m studies carried out on compounds **1a−f** provided evidence that both the PBD and polypyrrole components contribute to DNA stabilization in a synergistic manner.[20] These results revealed maximal DNA stabilization for the homologue containing three pyrrole units (**1c**), with a subsequent decline in ΔT_m values as the polypyrrole chain was extended further. In the present study, replacing the pyrrole units of **1c** with imidazole and thiazole heterocycles had different effects on ΔT_m depending on the number present and their position within the polyamide chain. For example, replacing the pyrrole at the PBD end of Py−Py−Py−PBD (**1c**) with an imidazole (i.e., Py−Py−Im−PBD, **3a**, Group 1) increased DNA binding affinity (21.1 °C versus 20.2 °C at 18 h). On the other hand, inclusion of a single imidazole in either the middle (Py−Im−Py−PBD, **3b**) or terminal position (Im−Py−Py−PBD, **3e**) reduced ΔT_m to 16.9 and 18.7 °C (after 18 h), respectively. The introduction of two (Py−Im−Im−PBD, **3c**; Im−Im−Py−PBD, **3d**; Im−Py−Im−PBD, **3f**, Group 2) or three (Im−Im−Im−PBD, **3g**, Group 3) imidazole units resulted in a progressive loss of binding affinity. Replacement of the central pyrrole of **1c** (Py−Py−Py−PBD) with a thiazole (**3i**, Py−Th−Py−PBD) was well tolerated, as indicated by the ΔT_m of 20.7 °C (at 18 h), the second highest ΔT_m shift observed and 0.5 °C higher than for the parent Py−Py−Py−PBD (**1c**). As with the imidazole replacements, inclusion of a thiazole in the other two possible positions (Py−Py−Th−PBD, **3h**; Th−Py−Py−PBD, **3l**) reduced the binding affinity, whereas replacement of all three pyrroles with thiazoles (Th−Th−Th−PBD, **3n**) afforded the lowest ΔT_m of all the conjugates (10.9 °C at 18 h). On the basis of these results, it was concluded that an imidazole next to the PBD (as in **3a**), or a thiophene in the central position (as in **3i**), improved DNA-binding affinity compared to the parent Py−Py−Py−PBD (**1c**).

Another interesting feature of the ΔT_m data for **3a** was that most of the induced effect upon CT-DNA melting appeared almost immediately, with ΔT_m values of 19.1, 19.8, and 21.1 °C at 0, 4, and 18 h, respectively, whereas the ΔT_m values for the parent tripyrrole analogue **1c** increased from 17.0 to 18.7 to

dx.doi.org/10.1021/jm4001852 | J. Med. Chem. XXXX, XXX, XXX−XXX

20.2 °C at 0, 4, and 18 h. This suggests that the C8-heterocyclic chain of **3a** may have a greater sequence selectivity and affinity for DNA than the tripyrrole chain of **1c**, resulting in the molecule being in the appropriate position for covalent bond formation immediately upon DNA minor-groove entry.

Although there is not a perfect correlation between cytotoxicity and thermal denaturation data for the conjugates examined, **3a** (Py−Py−Im−PBD), which provided the highest ΔT_m values and the greatest kinetic effect, also produced the lowest average GI_{50} value and the second lowest average LC_{50} and TGI values across the 60 cell lines of the NCI panel.

DNase I Footprinting Study. A semiautomated 96-well-plate DNase I footprinting assay was used to evaluate the sequence selectivity and DNA-binding affinity of the PBD−heterocycle conjugates. This methodology was developed by Hartley and co-workers, and differs from standard ^{32}P-radiolabeled DNase I footprinting in that radiolabels are replaced with infrared (IR) dyes and the gel visualized through dye detection using a diode laser.[29] The ligands were footprinted against 170 bp of the human Topo IIα promoter containing the ICB1 and ICB2 sequences, and the results were used to help determine which molecule to progress to the NF-Y functional assay (EMSA). The PBD dipyrrole conjugate **1b** was used as a positive control because of its known ability to bind to several CCAAT motifs and inhibit the binding of NF-Y to the promoter of DNA Topo IIα.[4] A range of concentrations of each member of the PBD−heterocycle library was incubated with the DNA fragment for 17 h at room temperature prior to DNase I cleavage, as this time period should allow complete covalent binding as reported in the literature[20] and was also consistent with the ΔT_m measurements. Compound **3a** exhibited the best DNA sequence recognition properties, and Figure 4 shows a comparison of the DNase I footprinting patterns for **1b** (Figure 4A) and **3a** (Figure 4B) against the 170 bp human Topo IIα promoter. The results indicate that although extension of the dipyrrole side chain of **1b** with an imidazole ring to afford **3a** had no effect on sequence selectivity with both the ICB1 and ICB2 sites specifically targeted on this particular DNA fragment, there was a small but significant difference in affinity between the two molecules for the ICB1 site. Whereas **1b** footprinted at both sites down to 1 μM (lane f), **3a** footprinted preferentially at the ICB2 site, losing affinity by 5-fold for the ICB1 site. Thus, the ICB1 footprint for **3a** was only visible down to 5 μM (lane g), whereas the footprint for ICB2 was observable down to the lower concentration of 1 μM (lane f). Therefore, **3a** was selected for evaluation in the electrophoretic mobility shift assay (EMSA).

Electrophoretic Mobility Shift Assay (EMSA). The relative preference of **3a** for the ICB2 site was further investigated using an EMSA study as described by Firth and co-workers,[30] based on a nuclear extract from NIH3T3 cells along with oligonucleotides containing the Topo IIα ICB1 (5′-CAGGG*ATTGG*CTGGT-3′) and ICB2 (5′-CTACG*ATTGG*-TTCTT-3′) sequences. The gels in Figure 5 show the effects of **3a** and **1b** on binding of the NF-Y transcription factor to the ICB1 and ICB2 sites. Both compounds inhibited NF-Y binding to the ICB2 site at 5 μM (Figure 5B). However, while **1b** inhibited NF-Y binding at ICB1 at 5 μM (Figure 5A), a 10-fold increase in concentration of **3a** (i.e., up to 50 μM) was required to inhibit NF-Y binding at this site. This result was consistent with the DNA footprinting data and confirms that, unlike **1b**, the extended PBD conjugate **3a** is capable of discriminating between the ICB1 and ICB2 sites.

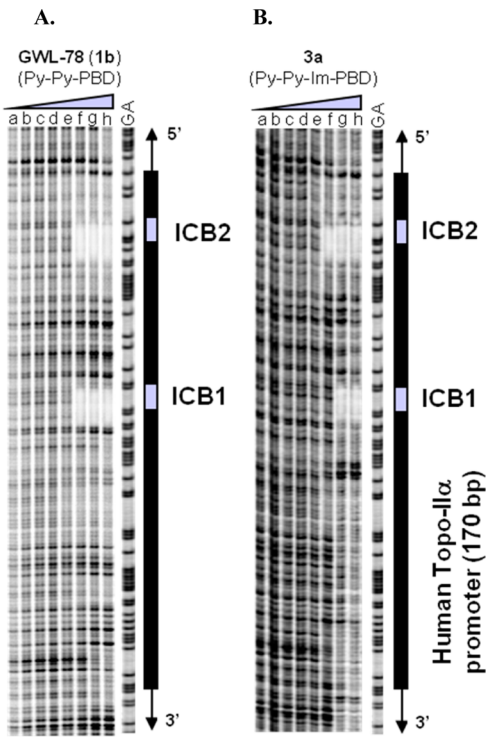

Figure 4. DNase I footprinting patterns for **1b** (A) and **3a** (B) at increasing concentrations against 170 base pairs (bp) of the human Topo-IIα promoter. Lanes a−h correspond to concentrations of 0, 0.0016, 0.008, 0.04, 0.2, 1, 5, and 25 μM, respectively. The guanine/adenine (GA) marker lanes were used for sequence identification.

In Vitro Cytotoxicity. The novel PBD conjugates were evaluated for in vitro cytotoxicity in the National Cancer Institute (NCI) 60-cell-line panel. The results (Table 1) show that, with the exception of **3g** and **3n**, most have significant cytotoxicity across the cell lines. Conjugate **3a** exhibited the lowest average GI_{50} value (1.3 nM) compared to all other PBD conjugates and the positive control **1c** (15 nM), and also had the second lowest TGI (24 nM) and LC_{50} (2.3 μM) values. From these data, it was possible to identify structure−activity relationships (SARs) with regard to cytotoxicity and DNA-binding affinity (i.e., induced ΔT_m), and this allowed the conjugates to be divided into three groups (Table 1) depending on the number of pyrrole rings in the C8-polyamide chain (i.e., 2, 1, and 0 pyrroles for Groups 1, 2 and 3, respectively). For example, replacement of the three pyrrole units of the C8-polyamide chain of **1c** with three imidazole (**3g**) or three thiazole (**3n**) rings (Group 3) caused a significant decrease in both cytotoxicity and induced ΔT_m. However, replacing the pyrrole rings of **1c** with either two (Group 2) or one (Group 1) imidazole or thiazole rings progressively increased both cytotoxicity and induced ΔT_m. Although the position of the pyrrole ring in the chain with respect to the two imidazole heterocycles in Group 2 (i.e., **3c**, **3d**, and **3f**) did not appear to have a significant effect on cytotoxicity or induced ΔT_m (although a central pyrrole ring, as in **3f**, appeared to improve induced ΔT_m slightly), in Group 1 two of the most cytotoxic analogues (**3a** and **3h**) and one with the highest induced ΔT_m (**3a**) have the nonpyrrolic heterocycle immediately adjacent to the PBD unit. Thus, the SAR data indicate that, in general, cytotoxicity correlates well with induced ΔT_m, and that to optimize both properties with respect to **1c**, just one pyrrole

dx.doi.org/10.1021/jm4001852 | J. Med. Chem. XXXX, XXX, XXX−XXX

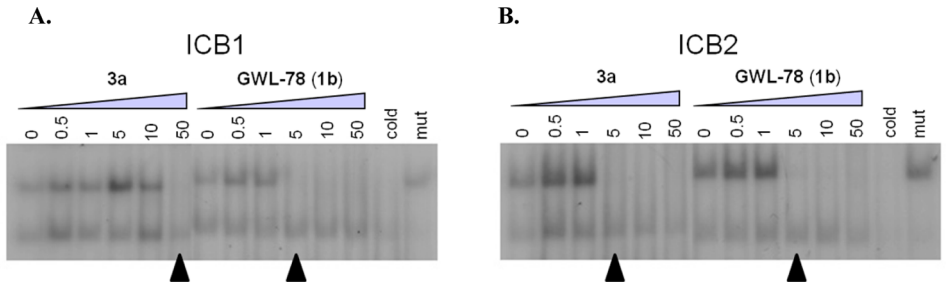

Figure 5. Results of an electrophoretic mobility shift assay (EMSA), showing the effect of **3a** and **1b** on NF-Y transcription factor binding at ICB1 (A) and ICB2 (B) sites at increasing concentrations (μM). The arrows indicate the lanes that correspond to the minimum concentrations at which the ligands displace the transcription factor. Unlabeled (cold) and mutated (mut) oligonucleotides were used as controls. The upper bands correspond to the protein/DNA complex.

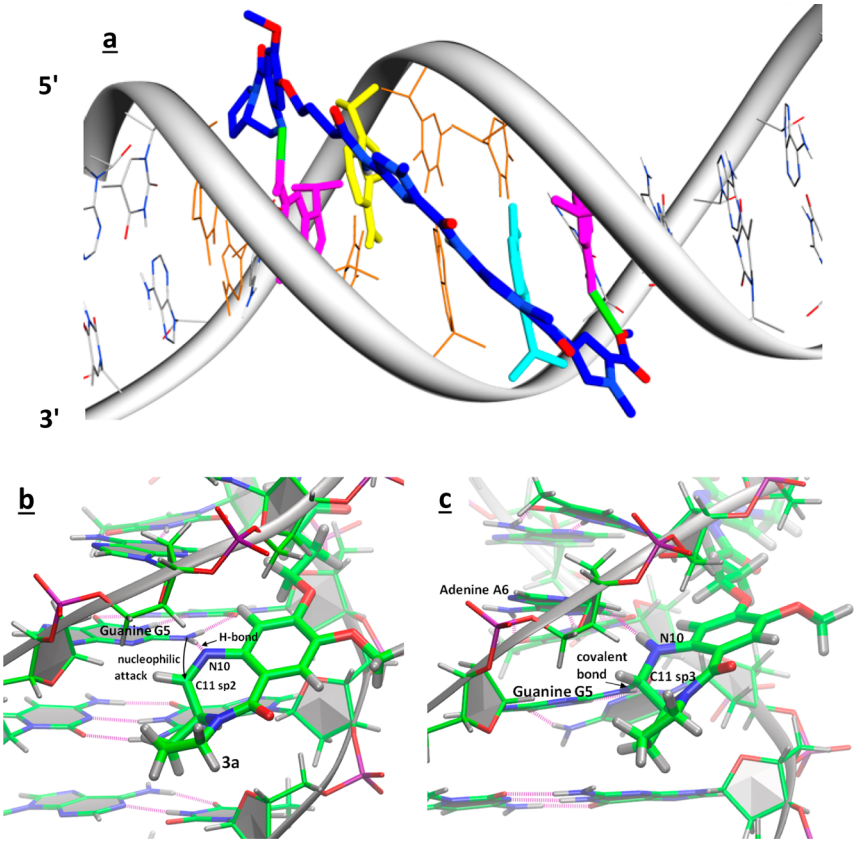

Figure 6. (a) Energy minimized structure of the adduct of **3a** noncovalently bound to the ICB2-containing DNA oligonucleotide (as used in the EMSA study). The A-ring of the PBD (left of model) is oriented toward the 3′-end of the duplex (i.e., A-Ring-3′) with the N10 of the PBD located in proximity to G5 (magenta), thus forming a hydrogen bond (green) between these two centers. A hydrogen bond (green) is also formed between the terminal OMe group (right of model) and G9 (magenta). Van der Waals interactions between the methylene chain and A6 (yellow) and between the second pyrrole and A23 (cyan) help retain the ligand in place. All DNA bonds are in wire representation with the DNA backbone (ribbon) in light gray and with **3a** in dark blue with some atom coloring. The ligand spans six base pairs, from C4 (orange) to G9 (magenta). (b) Detailed image of **3a** (thick sticks) noncovalently bound to DNA (thin sticks) with its C11-position adjacent to the G5 of the ICB2 oligonucleotide, showing the H-bond formation (magenta) between N10 of the PBD B-ring and the C2-NH_2 protons of G5, and the impending nucleophilic attack of the lone pair of the G5 C2-NH_2 on the C11 of the PBD C-ring. (c) Detailed image of **3a** covalently bound to G5 following formation of the covalent bond between the C11 of the PBD B-ring and the C2-NH_2 of G5. For images b and c, all bonds are shown in normal atom coloring.

should be replaced with either an imidazole next to the PBD (i.e., **3a**) or a thiazole in the central position (i.e., **3i**).

Molecular Modeling. To study the differences in binding affinities observed for **3a** toward the ICB1 and ICB2 sequences, a molecular mechanics modeling approach was used to investigate ligand behavior in the minor grooves of the oligonucleotides used in the EMSA study that contain the Topo IIα ICB1 (5′-$C_1A_2G_3G_4G_5A_6T_7T_8G_9G_{10}C_{11}$-$T_{12}G_{13}G_{14}T_{15}$-3′) and ICB2 (5′- $C_1T_2A_3C_4G_5A_6T_7T_8G_9G_{10}T_{11}$-$T_{12}C_{13}T_{14}T_{15}$-3′) target sequences. Although it is feasible for PBD molecules to orientate in either direction with respect to the covalently bound strand, we initially focused on the most likely models for inhibition of transcription factor binding with the ligand spanning six base pairs of the protein binding site (e.g., 5′-ATTGGC-3′ for ICB1, and 5′-ATTGGT-3′ for ICB2)[18] and oriented with the A-ring pointing toward the 3′-

dx.doi.org/10.1021/jm4001852 | J. Med. Chem. XXXX, XXX, XXX–XXX

end of the potentially covalently-modified strand (designated A-Ring-3′), the preferred orientation according to the literature.[8,20,25] In these models, guanine-5 (G5) was the most obvious base for alkylation in ICB2, and guanine-4 (G4) or G5 in ICB1, with a preference for the latter in ICB1 to provide maximum coverage of the protein binding site. Therefore, **3a** (in its N10-C11 imine form) was aligned in the minor groove in the center of each 15-mer duplex with the A-ring of the PBD moiety pointing toward the 3′-end of the strand most likely to be covalently modified,[8,20,25] and with the bulk of the molecule spanning six to seven base pairs of the inverted CAAT box sequence. Since the N10 atom of the PBD molecule in its N10-C11 imine form carries a lone pair of electrons (and thus a partial negative charge), and since the hydrogen atoms of the C2-amino group of G5 carry a partial positive charge, these two centers were initially placed close to each other on the basis that electrostatic attraction and/or H-bond formation would be important factors in the initial recognition process and would maintain them in proximity during the dynamics simulation.

Molecular dynamics simulations in explicit solvent and free energy calculations were then performed according to the method described. Following this, further dynamics experiments were carried out with **3a** in the same longitudinal orientation but covalently bound to G5 in both the ICB1 and ICB2 oligonucleotides, with an aminal bond formed between the C11-position of the B-ring of the PBD and the nitrogen of the exocyclic C2-NH_2 of G5, while maintaining a *S*-configuration at the PBD C11-position in accord with previously published studies.[8,20,25] Control simulations of the ICB1 and ICB2 duplexes devoid of ligand were also carried out, and plots were generated for any binding-induced variations in DNA conformation and minor-groove width over the course of the simulations (see Figures S3−S14 in Supporting Information). The initial noncovalently bound models showed that **3a** is snugly accommodated in the minor groove of each duplex host, with the heterocycles of the C8-polyamide side chain following the curvature of the groove toward the 3′-end of the potentially covalently modified strand (see Figure 6a for ICB2). These initial models also confirmed that **3a** spans six base pairs of the targeted sequences (i.e., ICB1, 5′-GGATTG-3′; ICB2, 5′-CGATTG-3′; G5 underlined). It is likely that such initial noncovalent positioning of the PBD moiety through electrostatic attraction and/or hydrogen bonding may be a factor in orientating the reacting groups prior to covalent bond formation by locating the lone pair of the C2-NH_2 nitrogen of G5 in proximity to the electrophilic C11-position of the PBD. This would facilitate nucleophilic attack of the C2-NH_2 followed by atomic rearrangement within the PBD molecule to allow protonation of N10 and sp^3 hybridization of the C11-position (Figures 6b,c). These models also confirmed that the orientation of the reacting groups and the directionality of nucleophilic attack should generate a *S*-configuration at the C11-position of the PBD in the adduct, consistent with previous NMR and X-ray modeling studies of the interaction of PBD molecules with DNA.[31,32] Crucially, the models predicted that an *R*-configuration at the C11-position of the PBD in the adducts would provide a highly unfavorable conformation for the PBD molecules within the DNA minor groove.

Additional modeling studies were undertaken to investigate other possible covalent adducts that could form on either strand in both the A-Ring-3′ or A-Ring-5′ orientations. In the case of ICB1, there are six potentially reacting guanines: G3, G4, G5 and G20 (A-Ring-3′) and G9 and G10 (A-Ring-5′) (Figure 7). Models of **3a**, **1c**, and **3k** bound to each reacting

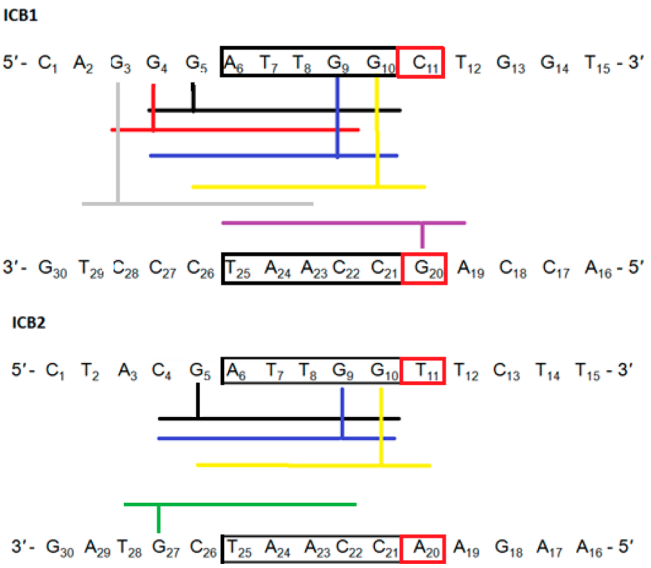

Figure 7. Schematic diagram showing all possible (A-Ring-3′ and A-Ring-5′) covalent adducts within the ICB1 (i.e., G3, G4, G5, G9, G10, and G20) and ICB2 (i.e., G5, G9, G10, and G27) transcription factor binding sites. **3a** is represented as a series of differently colored horizontal lines for each potential adduct which are drawn to scale with respect to base pair span. Vertical lines of the same color linking to guanine residues represent the covalent bond between the C11-position of the PBD and the C2-NH_2 group of the particular guanine. The identical CAAT box motifs (i.e., 5′-ATTGG-3′) of the ICB1 and ICB2 sequences are highlighted in black boxes, and the 3′-flanking residues, which differ, are highlighted in red boxes.

guanine of the ICB1 sequence showed identical hydrogen bonding patterns, with a greater number of hydrogen bonds formed with the PBD bound in the A-Ring-5′ compared to the A-Ring-3′ orientations. However, a single hydrogen bond was observed between the N10-H of the PBD and the ring nitrogen of a neighboring base (e.g., G5 or A6) when bound to G4 or G5, respectively. A hydrogen bond was also observed to form between the -OMe group of the terminal ester of **3a**, **1c**, and **3k** and the exocyclic amine of G4 and G5, when bound A-Ring-5′ to G9 or G10, respectively. This hydrogen bond is absent in the A-Ring-3′ direction and may explain the enhanced interactivity of the PBD−polyamide trimer structures (e.g., **3a**) compared to the PBD−polyamide dimeric molecules (e.g., **1c**) with both ICB1 and ICB2, as **1c** does not span the required number of bases to form this bond. A single hydrogen bond was also formed between N10-H of the PBD and A19 with the PBDs bound to G20 (A-Ring-3′) (Figures S1 and S2 in Supporting Information).

A similar modeling study was undertaken on ICB2, with **3a**, **1c**, and **3k** bound to each of the four potentially reacting guanines near the central binding sequence (i.e., G5, G9, G10, or G27; Figure 7). In the cases of G5, G9, and G10, an identical hydrogen bonding pattern for **3a**, **1c**, and **3k** was observed as for ICB1. However, when bound to G27, a single constant hydrogen bond between the N10-H of the PBD ring and the ring nitrogen of the adjacent G5 on the opposite stand was observed for 3a (Figure S2 in Supporting Information), whereas this hydrogen bonding interaction was absent in the case of **1c**. On closer inspection, this hydrogen bond occurred

dx.doi.org/10.1021/jm4001852 | J. Med. Chem. XXXX, XXX, XXX−XXX

because of increased van der Waal interactions between **3a** and the central -ATT- region of the binding sequence as a result of the enhanced curvature of the **3a** structure resulting from the absence of van der Waals repulsion between N3 of the imidazole group and adjacent functional groups, compared to pyrrole groups. In the case of **3k**, the equivalent hydrogen bond was transient throughout the simulation, and the ring nitrogens of the thiazole groups prevented the formation of favorable van der Waals interactions within the minor groove, thus leading to poorer accommodation compared to **3a**. These interactions are reflected in the free energy values and could also explain the slightly enhanced ΔT_m of **3a** compared to **1c**, and the preference of **3a** for ICB2 over ICB1. The calculated free energies of **3a** when bound noncovalently to the ICB1- and ICB2-containing oligonucleotides in the A-Ring-3′ orientation were found to be −56.8 and −63.6 kcal/mol, respectively, over the duration of the simulation. This suggested that noncovalent binding to the ICB2-containing duplex is favored by 6.8 kcal/mol, in accord with both the DNA footprinting (Figure 4) and EMSA (Figure 5) data.

Finally, a full analysis of the free energy of binding at all potential guanine sites using single snapshots of molecular dynamics simulations was undertaken. This involved studying snapshots of **3a**, **1c**, and **3k** with their N10 positions interacting with each potentially reacting guanine (G3, G4, G5, G9, G10, and G20 in the case of ICB1, and G5, G9, G10 and G27 in the case of ICB2), in an effort to identify favored reacting sites (Table 2). The average values shown in the table indicate that,

Table 2. Individual and Average Free Energies (kcal/mol) Calculated for 3a, 1c, and 3k in the Minor Groove of the ICB1 and ICB2 Sequences, with Their N10 Atoms Adjacent to Each Potentially Reacting Guanine

Reacting guanine	Py−Py−Im−PBD (**3a**)	Py−Py−Py−PBD (**1c**)	Th−Th−Py−PBD (**3k**)
ICB1 G3	−73.32	−71.26	−58.68
ICB1 G4	−70.66	−65.35	−59.84
ICB1 G5	−62.26	−69.15	−63.27
ICB1 G9	−67.16	−63.60	−63.15
ICB1 G10	−68.64	−63.44	−46.71
ICB1 G20	−69.51	−57.39	−51.79
Average value	−68.59	−65.03	−57.24
ICB2 G5	−68.82	−73.70	−44.42
ICB2 G9	−70.51	−64.05	−66.05
ICB2 G10	−72.69	−67.35	−60.31
ICB2 G27	−72.09	−69.67	−62.42
Average value	−71.03	−68.69	−58.30

based on average values across all possible adducts, **3a** has a preference for ICB2 (i.e., −71.03 kcal/mol) compared to ICB1 (−68.59). The equivalent values for **1c** (i.e., −68.69 and −65.03 kcal/mol for ICB2 and ICB1, respectively) and **3k** (i.e., −58.30 and −57.24 kcal/mol for ICB2 and ICB1, respectively) are higher but in the correct rank order (i.e., **1c** has a higher DNA thermal denaturation value than **3k**). Therefore, these results support the DNA thermal denaturation data and also the results of the footprinting and EMSA assays. This type of analysis, based on calculating the energies of every possible adduct at all binding sites, has not been applied to PBD adducts before, and the results suggest that it could be useful to predict the preferred binding sites of other PBD molecules.

CONCLUSIONS

A library of novel C8-linked PBD−heterocyclic polyamide conjugates (**3a−n**) has been synthesized and evaluated in DNA thermal denaturation, DNase I footprinting, EMSA, and cytotoxicity assays to provide SAR information relating the type and position of heterocyclic rings in the C8-polyamide side chain to the DNA-binding affinity and cytotoxicity. The results show that substituting the pyrrole ring immediately adjacent to the PBD unit in the known Py−Py−Py−PBD conjugate (**1c**) with an imidazole ring (i.e., Py−Py−Im−PBD, **3a**) enhances the induced ΔT_m shift with calf thymus DNA by approximately 1 °C. Furthermore, unlike the shorter PBD conjugate Py−Py−PBD (**1b**), DNA footprinting and EMSA data indicate that **3a** can discriminate between the ICB1 and ICB2 sequences, thereby inhibiting NF-Y binding at the ICB2 site at a 10-fold lower concentration than at ICB1. The results of free energy calculations support the preference of **3a** for ICB2, and suggest that their application to a full analysis of all possible adducts at a particular binding site could assist in the design of future generations of sequence-targeted molecules of this type.

Although the observed selectivity of **3a** for ICB2 versus ICB1 is small, these findings suggest that it may prove possible to design small-molecule inhibitors that can discriminate between different DNA recognition sites within a transcription factor family. Such molecules have potential as chemical biology tools to modulate transcription factor binding, and also as therapeutic agents across a number of disease types.

EXPERIMENTAL SECTION

Chemistry. Synthesis of PBD Conjugates 3a−n. Procedures for the synthesis of intermediates **6a−g**, **8a−n**, and the Alloc-THP-protected PBD conjugates **10a−n**, and analytical data for **1c**, are provided in Supporting Information.

General Alloc and THP Deprotection Procedure for the Synthesis of 3a−n. $Pd[PPh_3]_4$ (0.05 equiv) was added to a solution of the Alloc-THP-PBD−heterocycle conjugate (**10a−n**) and pyrrolidine (1.1 equiv) in dry CH_2Cl_2 (5 mL) under a N_2 atmosphere, and the reaction mixture was allowed to stir at room temperature for 1 h. The solvent was removed in vacuo and the residue purified using a preparative HPLC coupled to a mass-directed fraction collector. Pure fractions were combined and lyophilized to yield the product (**3a−n**) as a solid.

General Purification Procedure. Flash chromatography purification was performed using Merck Kieselgel 60 F254 silica gel. Extraction and chromatography solvents were purchased and used without further purification from Fisher Scientific (U.K.). All other chemicals and reagents were purchased from Sigma-Aldrich, Lancaster or BDH (U.K.). The purity of target compounds **3a−n** was assessed by analysis of their NMR, HRMS, and HPLC data.

^{1}H NMR Spectra. Data were acquired using a Bruker Avance 400 spectrometer operating at 400 MHz. Coupling constants are quoted in Hertz (Hz), and chemical shifts are reported in parts per million (ppm) downfield from tetramethylsilane. Spin multiplicities are described as s (singlet), br s (broad singlet), d (doublet), dd (doublet of doublets), t (triplet), q (quartet), p (pentuplet), or m (multiplet).

LC−MS Methodology. The HPLC system consisted of a Waters 2767 sample manager fitted with a 20 μL loop, a Waters 2996 PDA, and a Waters Micromass ZQ mass spectrometer utilizing electrospray ionization with scanning from 100 to 1500 Da in positive ion mode. The sample injection volume was 20 μL. Four different methods were used as follows:

Method 1. This method utilized a Luna 3 μm C8(2) column (100 mm × 4.6 mm) with a flow rate of 1.5 mL/min and a linear gradient solvent system (95:5 v/v solvent A/B at time 0 to 5:95 v/v A/B at 4 min after sample injection, then maintained at 5:95 v/v until 7 min). Solvent A was 0.1% v/v formic acid in water, and solvent B was 0.1%

dx.doi.org/10.1021/jm4001852 | J. Med. Chem. XXXX, XXX, XXX−XXX

v/v formic acid in acetonitrile. The electrospray mass spectrometer was operated in switching mode to obtain both positive and negative ion spectra.

Method 2. This method utilized the same column, flow rate, solvent systems and MS switching mode as for Method 1 but a different linear gradient: 95:5 v/v solvent A/B at time 0 to 5:95 v/v A/B at 3 min after sample injection, then maintained at 5:95 v/v until 5 min.

Methods 3 and 4. These Methods utilized Phenomenex Luna 5 μm C18(2) (250 mm × 4.6 mm) and Gemini 5 μm C18 (100 mm × 4.6 mm) columns, respectively. The solvent composition for both Methods was (A) 0.1% v/v formic acid in water and (B) 0.1% v/v formic acid in acetonitrile, with a flow rate of 1.5 mL/min. The gradient elution conditions for both Methods were: 95:5 v/v solvent A/B at time 0 to 5:95 v/v A/B at 18 min after sample injection, maintained at 5:95 v/v A/B until 22 min, reverted to 95:5 v/v A/B at 23 min, and then maintained at 95:5 v/v A/B until 30 min.

Analytical Data for PBD Conjugates 3a–i and 3k–n. Methyl 4-({4-[4-(7-Methoxy-5-oxo-2,3,5,11a-tetrahydro-5*H*-pyrrolo-[2,1-*c*][1,4]benzodiazepine-8-yloxy)butyrylamino]-1-methyl-1*H*-imidazole-2-carbonyl]amino)-1-methyl-1*H*-pyrrole-2-carbonyl]amino}-1-methyl-1*H*-pyrrole-2-carboxylate (3a). The Alloc-THP-PBD-imidazole-pyrrole-pyrrole conjugate **10a** (200 mg, 0.22 mmol) was deprotected as described in the general procedure to yield the imine product **3a** (45 mg, 29%). ^{1}H NMR (acetone-d_6): δ 9.38 (s, 1H, N-H), 9.37 (s,1H, N-H), 9.22 (s, 1H, N-H), 7.73 (d, 1H, J = 4.4 Hz, H-11), 7.50 (d, 1H, J = 1.9 Hz, Py-H), 7.47 (s, 1H, Im-H), 7.43 (s, 1H, H-6), 7.28 (d, 1H, J = 1.8 Hz, Py-H), 7.00 (d, 1H, J = 1.8 Hz, Py-H), 6.94 (d, 1H, J = 2.0 Hz, Py-H), 6.82 (s, 1H, H-9), 4.20 (m, 1H, side chain H-1), 4.10 (m, 1H, side chain H-1), 4.06 (s, 3H, O/N-CH_3), 4.00 (s, 3H, O/N-CH_3), 3.95 (s, 3H, O/N-CH_3), 3.91 (s, 3H, O/N-CH_3), 3.76 (s, 3H, O/N-CH_3), 3.68 (m, 2H, H-11a, H-3), 3.44 (m, 1H, H-3), 2.64 (m, 2H, side chain H-3), 2.33 (m, 2H, H-1), 2.19 (m, 2H, side chain H-2), 2.09 (s, 2H, H-2). LCMS: method 1, t_R = 2.67 min; method 3, t_R = 10.22 min; method 4, t_R = 8.35 min. MS, m/z (ES+): 714 ($M^\bullet$ + H^+). Calcd for $C_{35}H_{39}N_9O_8$, 714.2994. Found, 714.3011 ($M^\bullet$ + H^+).

Methyl 4-({4-[4-(7-Methoxy-5-oxo-2,3,5,11a-tetrahydro-5*H*-pyrrolo[2,1-*c*][1,4]benzodiazepine-8-yloxy)butyrylamino]-1-methyl-1*H*-pyrrole-2-carbonyl]amino)-1-methyl-1*H*-imidazole-2-carbonyl]amino}-1-methyl-1*H*-pyrrole-2-carboxylate (3b). The Alloc-THP-PBD-pyrrole-imidazole-pyrrole conjugate **10b** (260 mg, 0.29 mmol) was deprotected as described in the general procedure to yield the imine product **3b** (34 mg, 16%). ^{1}H NMR (acetone-d_6): δ 9.88 (s, 1H, N-H), 9.69 (s, 1H, N-H), 9.53 (s, 1H, N-H), 7.76 (d, 1H, J = 4.4 Hz, H-11), 7.60 (d, 1H, J = 1.1 Hz, Py-H), 7.50 (s, 1H, Im-H), 7.43 (s, 1H, H-6), 7.19 (d, 1H, J = 2.2 Hz, Py-H), 7.01 (d, 1H, J = 1.5 Hz, Py-H), 6.98 (d, 1H, J = 1.3 Hz, Py-H), 6.83 (s, 1H, H-9), 4.21 (m, 2H, side chain H-1), 4.06 (s, 3H, O/N-CH_3), 3.90 (s, 6H, O/N-CH_3), 3.88 (s, 3H, O/N-CH_3), 3.76 (s, 3H, O/N-CH_3), 3.67 (m, 2H, H-11a, H-3), 3.50 (m, 1H, H-3), 2.53 (m, 2H, side chain H-3), 2.36 (m, 2H, H-1), 2.19 (m, 2H, side chain H-2), 2.09 (s, 2H, H-2). LCMS: method 1, t_R = 2.65 min; method 3, t_R = 10.18 min; method 4, t_R = 8.32 min. MS, m/z (ES+): 714 ($M^\bullet$ + H^+). Calcd for $C_{35}H_{39}N_9O_8$, 714.2994. Found, 714.2999 ($M^\bullet$ + H^+).

Methyl 4-({4-[4-(7-Methoxy-5-oxo-2,3,5,11a-tetrahydro-5*H*-pyrrolo[2,1-*c*][1,4]benzodiazepine-8-yloxy)butyrylamino]-1-methyl-1*H*-imidazole-2-carbonyl]amino)-1-methyl-1*H*-imidazole-2-carbonyl]amino}-1-methyl-1*H*-pyrrole-2-carboxylate (3c). The Alloc-THP-PBD-imidazole-imidazole-pyrrole conjugate **10c** (130 mg, 0.14 mmol) was deprotected as described in the general procedure to afford imine product **3c** (28 mg, 28%). ^{1}H NMR (acetone-d_6): δ 9.71 (s, 1H, N-H), 9.42 (s, 1H, N-H), 9.05 (s, 1H, N-H), 8.02 (s, 1H, Im-H), 7.73 (d, 1H, J = 4.4 Hz, H-11), 7.56 (s, 1H, Im-H), 7.50 (d, 1H, J = 5.0 Hz, Py-H), 7.42 (s, 1H, H-6), 7.18 (d, 1H, J = 1.2 Hz, Py-H), 6.83 (s, 1H, H-9), 4.14 (m, 2H, side chain H-1), 4.10 (s, 3H, O/N-CH_3), 4.07 (s, 3H, O/N-CH_3), 3.94 (s, 3H, O/N-CH_3), 3.92 (s, 3H, O/N-CH_3), 3.78 (s, 3H, O/N-CH_3), 3.67 (m, 1H, H-11a), 3.52 (m, 1H, H-3), 3.39 (m, 1H, H-3), 2.52 (m, 2H, side chain H-3), 2.31 (m, 2H, H-1), 2.21 (m, 2H, side chain H-2), 2.09 (s, 2H, H-2). LCMS: method 1, t_R = 2.70 min; method 3, t_R = 10.45 min; method 4, t_R = 8.57 min. MS, m/z (ES+): 715 ($M^\bullet$ + H^+). Calcd for $C_{34}H_{38}N_{10}O_8$, 715.2974. Found, 715.2956 ($M^\bullet$ + H^+).

Ethyl 4-({4-[4-(7-Methoxy-5-oxo-2,3,5,11a-tetrahydro-5*H*-pyrrolo[2,1-*c*][1,4]benzodiazepine-8-yloxy)butyrylamino]-1-methyl-1*H*-pyrrole-2-carbonyl]amino)-1-methyl-1*H*-imidazole-2-carbonyl]amino}-1-methyl-1*H*-imidazole-2-carboxylate (3d). The Alloc-THP-PBD-pyrrole-imidazole-imidazole conjugate **10d** (145 mg, 0.16 mmol) was deprotected as described in the general procedure to yield the imine product **3d** (16 mg, 14%). ^{1}H NMR (acetone-d_6): δ 9.46 (s, 1H, N-H), 9.29 (s, 1H, N-H), 9.19 (s, 1H, N-H), 7.75 (d, 1H, J = 4.4 Hz, H-11), 7.59 (s, 1H, Im-H), 7.58 (s, 1H, Im-H), 7.42 (s, 1H, H-6), 7.36 (d, 1H, J = 1.7 Hz, Py-H), 6.99 (d, 1H, J = 1.7 Hz, Py-H), 6.81 (s, 1H, H-9), 4.34 (q, 2H, J = 7.1 Hz, OCH_2CH$_3$), 4.15 (m, 2H, side chain H-1), 4.10 (s, 3H, O/N-CH_3), 4.04 (s, 3H, O/N-CH_3), 3.94 (s, 3H, O/N-CH_3), 3.87 (s, 3H, O/N-CH_3), 3.68 (m, 1H, H-11a), 3.58 (m, 1H, H-3), 3.46 (m, 1H, H-3), 2.54 (m, 2H, side chain H-3), 2.36 (m, 2H, H-1), 2.21 (m, 2H, side chain H-2), 2.09 (m, 2H, H-2), 1.36 (t, 3H, J = 7.1 Hz, OCH$_2$CH_3). LCMS: method 1, t_R = 2.62 min; method 3, t_R = 9.98 min; method 4, t_R = 8.17 min. MS, m/z (ES+): 729 ($M^\bullet$ + H^+). Calcd for $C_{35}H_{40}N_{10}O_8$, 729.3104. Found, 729.3115 ($M^\bullet$ + H^+).

Ethyl 4-({4-[4-(7-Methoxy-5-oxo-2,3,5,11a-tetrahydro-5*H*-pyrrolo[2,1-*c*][1,4]benzodiazepine-8-yloxy)butyrylamino]-1-methyl-1*H*-pyrrole-2-carbonyl]amino)-1-methyl-1*H*-pyrrole-2-carbonyl]amino}-1-methyl-1*H*-imidazole-2-carboxylate (3e). The Alloc-THP-PBD-pyrrole-imidazole conjugate **10e** (210 mg, 0.23 mmol) was deprotected as described in the general procedure to yield the imine product **3e** (28 mg, 17%). ^{1}H NMR (acetone-d_6) δ 9.40 (s, 1H, N-H), 9.29 (s, 1H, N-H), 9.07 (s, 1H, N-H), 8.15 (s, 1H, Im-H), 7.74 (d, 1H, J = 4.4 Hz, H-11), 7.59 (s, 1H, H-9), 7.48 (d, 1H, J = 1.6 Hz, Py-H), 7.42 (d, 1H, J = 2.1 Hz, Py-H), 7.16 (d, 1H, J = 1.6 Hz, Py-H), 6.83 (d, 2H, J = 1.8 Hz, Py-H, H-6), 4.33 (q, 2H, J = 7.1 Hz, OCH_2CH$_3$), 4.13 (m, 2H, side chain H-1), 4.01 (s, 3H, O/N-CH_3), 3.96 (s, 3H, O/N-CH_3), 3.91 (s, 3H, O/N-CH_3), 3.87 (s, 3H, O/N-CH_3), 3.69 (m, 2H, H-11a, H-3), 3.47 (m, 1H, H-3), 2.55 (m, 2H, side chain H-3), 2.36 (m, 2H, H-1), 2.15 (m, 2H, side chain H-2), 2.09 (m, 2H, H-2), 1.37 (t, 3H, J = 7.1 Hz, OCH$_2$CH_3). LCMS: method 1, t_R = 2.60 min; method 3, t_R = 9.80 min; method 4, t_R = 7.97 min. MS, m/z (ES+): 728 ($M^\bullet$ + H^+). Calcd for $C_{36}H_{41}N_9O_8$, 728.3151. Found, 728.3151 ($M^\bullet$ + H^+).

Ethyl 4-({4-[4-(7-Methoxy-5-oxo-2,3,5,11a-tetrahydro-5*H*-pyrrolo[2,1-*c*][1,4]benzodiazepine-8-yloxy)butyrylamino]-1-methyl-1*H*-imidazole-2-carbonyl]amino)-1-methyl-1*H*-pyrrole-2-carbonyl]amino}-1-methyl-1*H*-imidazole-2-carboxylate (3f). The Alloc-THP-PBD-imidazole-pyrrole-imidazole conjugate **10f** (120 mg, 0.13 mmol) was deprotected as described in the general procedure to yield the imine product **3f** (26 mg, 27%). ^{1}H NMR (acetone-d_6): δ 9.52 (s, 1H, N-H), 9.42 (s, 1H, N-H), 9.27 (s, 1H, N-H), 7.74 (d, 1H, J = 4.4 Hz, H-11), 7.60 (s, 1H, Im-H), 7.49 (d, 1H, J = 1.7 Hz, Py-H), 7.44 (s, 1H, Im-H), 7.42 (s, 1H, H-6), 7.27 (d, 1H, J = 1.8 Hz, Py-H), 6.82 (s, 1H, H-9), 4.33 (q, 2H, J = 7.1 Hz, OCH_2CH$_3$), 4.16 (m, 1H, side chain H-1), 4.06 (m, 1H, side chain H-1), 4.02 (s, 3H, O/N-CH_3), 3.98 (s, 3H, O/N-CH_3), 3.88 (s, 3H, O/N-CH_3), 3.80 (s, 3H, O/N-CH_3), 3.69 (m, 2H, H-11a, H-3), 3.48 (m, 1H, H-3), 2.65 (m, 2H, side chain H-3), 2.35 (m, 2H, H-1), 2.18 (m, 2H, side chain H-2), 2.09 (s, 2H, H-2), 1.38 (t, 3H, J = 7.1 Hz, OCH$_2$CH_3). LCMS: method 1, t_R = 2.60 min; method 3, t_R = 9.22 min; method 4, t_R = 8.12 min. MS, m/z (ES+): 729 ($M^\bullet$ + H^+). Calcd for $C_{35}H_{40}N_{10}O_8$, 729.3104. Found, 729.3075 ($M^\bullet$ + H^+).

Ethyl 4-({4-[4-(7-Methoxy-5-oxo-2,3,5,11a-tetrahydro-5*H*-pyrrolo[2,1-*c*][1,4]benzodiazepine-8-yloxy)butyrylamino]-1-methyl-1*H*-imidazole-2-carbonyl]amino)-1-methyl-1*H*-imidazole-2-carbonyl]amino}-1-methyl-1*H*-imidazole-2-carboxylate (3g). The Alloc-THP-PBD-imidazole-imidazole-imidazole conjugate **10g** (135 mg, 0.15 mmol) was deprotected using the general procedure to give imine product **3g** (24 mg, 22%). ^{1}H NMR (DMSO-d_6): δ 10.53 (m, 1H, N-H), 10.16 (s, 1H, N-H), 9.54 (s, 1H, N-H), 7.78 (d, 1H, J = 4.4 Hz, H-11), 7.71 (s, 1H, Im-H), 7.64 (s, 1H, Im-H), 7.54 (s, 1H, Im-H), 7.32 (s, 1H, H-6), 6.83 (s, 1H, H-9), 4.29 (q, 2H, J = 7.1 Hz, OCH_2CH$_3$), 4.16 (m, 2H, side chain H-1), 4.00 (s, 3H, O/N-CH_3), 3.98 (s, 3H, O/N-CH_3), 3.95 (s, 3H, O/N-CH_3),

dx.doi.org/10.1021/jm4001852 | J. Med. Chem. XXXX, XXX, XXX–XXX

3.82 (s, 3H, O/N-CH_3), 3.67 (m, 2H, H-11a, H-3), 3.59 (m, 1H, H-3), 2.42 (m, 2H, side chain H-3), 2.33 (m, 2H, H-1), 2.04 (m, 2H, side chain H-2), 1.93 (m, 2H, H-2), 1.31 (t, 3H, J = 7.1 Hz, OCH_2CH_3). LCMS: method 1, t_R = 2.62 min; method 3, t_R = 10.12 min; method 4, t_R = 8.28 min. MS, m/z (ES+): 730 ($M^\bullet + H^+$). Calcd for $C_{34}H_{39}N_{11}O_8$, 730.3056. Found, 730.3070 ($M^\bullet + H^+$).

Methyl 4-({4-[4-(7-Methoxy-5-oxo-2,3,5,11a-tetrahydro-5*H*-pyrrolo[2,1-*c*][1,4]benzodiazepine-8-yloxy)butyrylamino]-thiazole-4-carbonyl]amino)-1-methyl-1*H*-pyrrole-2-carbonyl]-amino}-1-methyl-1*H*-pyrrole-2-carboxylate (3h). The Alloc-THP-PBD-thiazole-pyrrole-pyrrole conjugate **10h** (130 mg, 0.14 mmol) was deprotected as described in the general procedure to yield the imine product **3h** (37 mg, 37%). ^{1}H NMR (acetone-d_6): δ 11.19 (s, 1H, N−H), 9.34 (s, 1H, N-H), 9.13 (s, 1H, N-H), 7.81 (s, 1H, Thz-H), 7.74 (d, 1H, J = 4.4 Hz, H-11), 7.50 (d, 1H, J = 1.9 Hz, Py-H), 7.45 (s, 1H, H-6), 7.31 (d, 1H, J = 1.6 Hz, Py-H), 6.99 (d, 1H, J = 1.7 Hz, Py-H), 6.93 (d, 1H, J = 1.9 Hz, Py-H), 6.82 (s, 1H, H-9), 4.14 (m, 2H, side chain H-1), 3.94 (s, 3H, O/N-CH_3), 3.91 (s, 3H, O/N-CH_3), 3.84 (s, 3H, O/N-CH_3), 3.76 (s, 3H, O/N-CH_3), 3.68 (m, 2H, H-11a, H-3), 3.44 (m, 1H, H-3), 2.34 (m, 2H, side chain H-3), 2.27 (m, 2H, H-1), 2.21 (m, 2H, side chain H-2), 2.09 (s, 2H, H-2). LCMS: method 1, t_R = 2.70 min; method 3, t_R = 10.32 min; method 4, t_R = 8.47 min. MS, m/z (ES+): 717 ($M^\bullet + H^+$). Calcd for $C_{34}H_{36}N_8O_8S$, 717.2449. Found, 717.2441 ($M^\bullet + H^+$).

Methyl 4-({4-[4-(7-Methoxy-5-oxo-2,3,5,11a-tetrahydro-5*H*-pyrrolo[2,1-*c*][1,4]benzodiazepine-8-yloxy)butyrylamino]-1-methyl-1*H*-pyrrole-2-carbonyl]amino)thiazole-4-carbonyl]-amino}-1-methyl-1*H*-pyrrole-2-carboxylate (3i). The Alloc-THP-PBD-pyrrole-thiazole-pyrrole conjugate **10i** (0.125 g, 0.14 mmol) was deprotected as described in the general procedure to yield the imine product **3i** (0.035 g, 35%). ^{1}H NMR (acetone-d_6) δ 11.07 (s, 1H, N-H), 9.25 (s, 1H, N-H), 9.23 (s, 1H, N-H), 7.81 (s, 1H, Thz-H), 7.75 (d, 1H, J = 4.4 Hz, H-11), 7.55 (d, 1H, J = 1.6 Hz, Py-H), 7.45 (d, 1H, J = 1.2 Hz, Py-H), 7.43 (s, 1H, H-6), 7.27 (d, 1H, J = 1.4 Hz, Py-H), 6.98 (d, 1H, J = 1.9 Hz, Py-H), 6.81 (s, 1H, H-9), 4.15 (m, 2H, side chain H-1), 3.98 (s, 3H, O/N-CH_3), 3.92 (s, 3H, O/N-CH_3), 3.88 (s, 3H, O/N-CH_3), 3.85 (s, 3H, O/N-CH_3), 3.68 (m, 1H, H-11a), 3.59 (m, 1H, H-3), 3.46 (m, 1H, H-3), 2.55 (m, 2H, side chain H-3), 2.36 (m, 2H, H-1), 2.18 (m, 2H, side chain H-2), 2.09 (s, 2H, H-2). LCMS: method 1, t_R = 2.68 min; method 3, t_R = 10.42 min; method 4, t_R = 8.62 min. MS, m/z (ES+): 717 ($M^\bullet + H^+$). Calcd for $C_{34}H_{36}N_8O_8S$, 717.2449. Found, 717.2464 ($M^\bullet + H^+$).

Ethyl 4-({4-[4-(7-Methoxy-5-oxo-2,3,5,11a-tetrahydro-5*H*-pyrrolo[2,1-*c*][1,4]benzodiazepine-8-yloxy)butyrylamino]-1-methyl-1*H*-pyrrole-2-carbonyl]amino)thiazole-4-carbonyl]-amino}thiazole-4-carboxylate (3k). The Alloc-THP-PBD-pyrrole-thiazole-thiazole conjugate **10k** (90 mg, 0.10 mmol) was deprotected as described in the general procedure to yield the imine product **3k** (6 mg, 8%). ^{1}H NMR (acetone-d_6): δ 9.28 (s, 2H, N-H), 8.23 (s, 1H, N-H), 8.09 (s, 1H, Thz-H), 8.04 (s, 1H, Thz-H), 7.75 (d, 1H, J = 4.4 Hz, H-11), 7.50 (d, 1H, J = 1.8 Hz, Py-H), 7.42 (s, 1H, H-6), 7.29 (d, 1H, J = 1.5 Hz, Py-H), 6.82 (s, 1H, H-9), 4.34 (q, 2H, J = 7.1 Hz, OCH_2CH_3), 4.16 (m, 2H, side chain H-1), 4.00 (s, 3H, O/N-CH_3), 3.88 (s, 3H, O/N-CH_3), 3.71 (m, 1H, H-11a), 3.59 (m, 1H, H-3), 3.46 (m, 1H, H-3), 2.56 (m, 2H, side chain H-3), 2.36 (m, 2H, H-1), 2.20 (m, 2H, side chain H-2), 2.09 (m, 2H, H-2), 1.37 (t, 3H, J = 7.1 Hz, OCH_2CH_3). LCMS: method 1, t_R = 2.95 min; method 3, t_R = 11.67 min; method 4, t_R = 9.72 min. MS, m/z (ES+): 735 ($M^\bullet + H^+$). Calcd for $C_{33}H_{34}N_8O_8S_2$, 735.2014. Found, 735.1989 ($M^\bullet + H^+$).

Ethyl 4-({4-[4-(7-Methoxy-5-oxo-2,3,5,11a-tetrahydro-5*H*-pyrrolo[2,1-*c*][1,4]benzodiazepine-8-yloxy)butyrylamino]-1-methyl-1*H*-pyrrole-2-carbonyl]amino)-1-methyl-1*H*-pyrrole-2-carbonyl]amino}-thiazole-4-carboxylate (3l). The Alloc-THP-PBD-pyrrole-pyrrole-thiazole conjugate **10l** (200 mg, 0.22 mmol) was deprotected as described in the general procedure to yield the imine product **3l** (9 mg, 6%). ^{1}H NMR (acetone-d_6): δ 10.88 (s, 1H, N-H), 9.46 (s, 1H, N-H), 9.07 (s, 1H, N-H), 7.93 (s, 1H, Thz-H), 7.75 (d, 1H, J = 4.4 Hz, H-11), 7.61 (d, 1H, J = 1.6 Hz, Py-H), 7.43 (d, 2H, J = 2.3 Hz, Py-H, H-6), 7.16 (d, 1H, J = 1.7 Hz, Py-H), 6.85 (d, 1H, J = 1.8 Hz, Py-H), 6.81 (s, 1H, H-9), 4.32 (q, 2H, J = 7.1 Hz, OCH_2CH_3), 4.14 (m, 2H, side chain H-1), 4.02 (s, 3H, O/N-CH_3), 3.99 (s, 3H, O/N-CH_3), 3.92 (s, 3H, O/N-CH_3), 3.69 (m, 2H, H-11a, H-3), 3.47 (m, 1H, H-3), 2.54 (m, 2H, side chain H-3), 2.36 (m, 2H, H-1), 2.21 (m, 2H, side chain H-2), 2.09 (s, 2H, H-2), 1.36 (t, 3H, J = 7.1 Hz, OCH_2CH_3). LCMS: method 1, t_R = 2.85 min; method 3, t_R = 11.05 min; method 4, t_R = 9.10 min. MS, m/z (ES+): 731 ($M^\bullet + H^+$). Calcd for $C_{35}H_{38}N_8O_8S$, 731.2606. Found, 731.2603 ($M^\bullet + H^+$).

Ethyl 4-({4-[4-(7-Methoxy-5-oxo-2,3,5,11a-tetrahydro-5*H*-pyrrolo[2,1-*c*][1,4]benzodiazepine-8-yloxy)butyrylamino]-thiazole-4-carbonyl]amino)-1-methyl-1*H*-pyrrole-2-carbonyl]-amino}thiazole-4-carboxylate (3m). The Alloc-THP-PBD-thiazole-pyrrole-thiazole conjugate **10m** (140 mg, 0.16 mmol) was deprotected as described in the general procedure to yield the imine product **3m** (9 mg, 8%). ^{1}H NMR (acetone-d_6): δ 11.28 (s, 1H, N-H), 10.95 (s, 1H, N-H), 9.30 (s, 1H, N-H), 7.95 (s, 1H, Thz-H), 7.84 (s, 1H, Thz-H), 7.75 (d, 1H, J = 4.4 Hz, H-11), 7.66 (d, 1H, J = 1.7 Hz, Py-H), 7.50 (d, 1H, J = 1.8 Hz, Py-H), 7.43 (s, 1H, H-6), 6.83 (s, 1H, H-9), 4.33 (q, 2H, J = 7.1 Hz, OCH_2CH_3), 4.21 (m, 2H, side chain H-1), 4.03 (s, 3H, O/N-CH_3), 3.87 (m, 3H, O/N-CH_3), 3.70 (m, 1H, H-11a), 3.58 (m, 1H, H-3), 3.50 (m, 1H, H-3), 2.53 (m, 2H, side chain H-3), 2.36 (m, 2H, H-1), 2.23 (m, 2H, side chain H-2), 2.09 (m, 2H, H-2), 1.36 (t, 3H, J = 7.1 Hz, OCH_2CH_3). LCMS: method 1, t_R = 2.88 min; method 3, t_R = 11.23 min; method 4, t_R = 9.33 min. MS, m/z (ES+): 735 ($M^\bullet + H^+$). Calcd for $C_{33}H_{34}N_8O_8S_2$, 735.2014. Found, 735.2026 ($M^\bullet + H^+$).

Ethyl 4-({4-[4-(7-Methoxy-5-oxo-2,3,5,11a-tetrahydro-5*H*-pyrrolo[2,1-*c*][1,4]benzodiazepine-8-yloxy)butyrylamino]-thiazole-4-carbonyl]amino)thiazole-4-carbonyl]amino}-thiazole-4-carboxylate (3n). The Alloc-THP-PBD-thiazole-thiazole-thiazole conjugate **10n** (208 mg, 0.23 mmol) was deprotected according to the general procedure to yield **3n** (20 mg, 12%). ^{1}H NMR (acetone-d_6): δ 11.09 (s, 1H, N-H), 9.73 (s,1H, N-H), 9.57 (s, 1H, N-H), 8.12 (s, 1H, Thz-H), 8.05 (s, 1H, Thz-H), 7.72 (d, 1H, J = 4.4 Hz, H-11), 7.68 (s, 1H, Thz-H), 7.41 (s, 1H, H-6), 6.96 (s, 1H, H-9), 4.34 (q, 2H, J = 7.1 Hz, OCH_2CH_3), 4.08 (m, 1H, side chain H-1), 3.93 (m, 1H, side chain H-1), 3.87 (s, 3H, O/N-CH_3), 3.78 (m, 1H, H-11a), 3.54 (m, 1H, H-3), 3.44 (m, 1H, H-3), 2.52 (m, 2H, side chain H-3), 2.36 (m, 2H, H-1), 2.21 (m, 2H, side chain H-2), 2.09 (m, 2H, H-2), 1.36 (t, 1H, J = 7.1 Hz, OCH_2CH_3). LCMS: method 1, t_R = 2.98 min; method 3, t_R = 12.0 min; method 4, t_R = 10.07 min. MS, m/z (ES+): 739 ($M^\bullet + H^+$). Calcd for $C_{31}H_{30}N_8O_8S_3$, 739.1422. Found, 739.1443 ($M^\bullet + H^+$).

Cytotoxicity Evaluation (NCI 60-Cell-Line Screen). Compounds **3a**−**i** and **3k**−**n** were screened in a similar manner to **1c**[20] in the NCI 60 human tumor cell line panel. The screening protocol and detailed results for **3a** are provided in Supporting Information.

Thermal Denaturation Studies. The PBD−heterocycle conjugates were subjected to DNA thermal melting (denaturation) studies using double-stranded calf thymus DNA (CT-DNA, type I, highly polymerized sodium salt; 42% G + C [Sigma]) at a fixed concentration of 100 μM (in DNAp, equivalent to 50 μM in bp), quantified using an extinction coefficient of 6600 (M phosphate)$^{-1}$ cm^{-1} at 260 nm.[33,34] Heating was applied at a rate of 1 °C/min in the 50−99 °C temperature range, with optical and temperature data sampling at 100 ms intervals. A separate experiment was carried out using buffer alone, and this baseline was subtracted from each DNA melting curve before data treatment. Experiments were conducted in triplicate.[33,34]

Solutions were prepared in pH 7.00 ± 0.01 aqueous buffer containing 10 mM NaH_2PO_4/Na_2HPO_4 and 1 mM Na_2EDTA (all AnalaR grade). Working solutions containing CT-DNA and the test compound (fixed 5 μM) were incubated at 37.0 ± 0.1 °C for 0−72 h using a Grant GD120 water bath.

Samples were monitored at 260 nm using a Cary 4000 UV−visible spectrophotometer fitted with a Peltier heating accessory. A precision probe calibrated to ±0.01 °C in the −10 to +120 °C range was used for temperature measurements. Heating was applied at a rate of 1 °C/min in the 50−99 °C temperature range, with optical and temperature data sampling at 100 ms intervals. A separate experiment was carried out using buffer alone, and this baseline was subtracted from each DNA melting curve before data treatment. Optical data were imported into the Origin 5 program (MicroCal Inc./GE Healthcare, North-

dx.doi.org/10.1021/jm4001852 | J. Med. Chem. XXXX, XXX, XXX−XXX

ampton, MA) for analysis. DNA helix → coil transition temperatures (T_m) were determined at the midpoint of the normalized melting profiles. Results for each compound are shown as the mean ± standard deviation from at least three determinations. Ligand-induced alterations in DNA melting behavior (ΔT_m) are given by $\Delta T_m = T_m$(DNA + ligand) − T_m(DNA), where the T_m value determined for native CT-DNA is 67.82 ± 0.07 °C (averaged from ∼110 runs). Working solutions of the test compounds contained ≤0.3% v/v DMSO, and T_m results were corrected for the effects of DMSO cosolvent using a linear correction term determined for calibration mixtures. Other [ligand]/[DNAp] molar ratios were examined for **3b** and **3c** to ensure that the fixed 5:100 or 20:100 ratios used for comparative assays did not result in saturation of the host DNA duplex.

For kinetic experiments, working DNA−ligand mixtures incubated at 37 °C were evaluated after fixed time intervals of 0 h (i.e., no incubation), 4 h, and 18 h.

Footprinting Assay. The protocol for the DNase I footprinting experiments using IR dyes has been previously described, together with the analytical procedure.[29] Briefly, the 170 bp of the human Topo IIα promoter containing ICB1 and ICB2 was amplified by PCR from human genomic DNA (Promega) using primers TIIA-F and TIIA-R. The resulting fragment was ligated into the pGEM-T Easy plasmid vector using a commercial kit (Promega). Plasmid containing the Topo IIα fragment was amplified and purified using a midiprep purification kit (Qiagen). IR700 dye (LI-COR Biosciences) end-labeled DNA was produced in 48 × 25 μL reactions by standard *Taq* (Sigma) PCR amplification from the plasmid template. The IR700 end-labeled DNA concentration was estimated by measuring optical density both at 260 nm wavelength (for DNA) and at 685 nm (for IR700 dye). DNA product was then diluted with 0.1 mM Tris-HCl, pH 8.5, to give a 100 nM stock, and this was stored at −20 °C. In a polypropylene 96-well plate (Eppendorf), 50 μL drug−DNA mixtures were prepared against the IR700 end-labeled DNA target. The conjugate ligands were incubated with DNA at eight concentrations: 0, 1.6, 8, 40, 200, 1000, 5000, and 25 000 nM. The drug dilutions (0.5 mM, 100 μM, 20 μM, 4 μM, 0.8 μM, 160 nM, and 32 nM) were prepared in 100% DMSO at 20 × final concentration, allowing 2.5 μL to be added to each mixture, providing a final mix of 5% v/v DMSO, 50 mM KCl, 20 mM Tris-HCl, pH 7.5, 1 mM $MgCl_2$, 0.5 mM DTT, and 4 nM IR700 end-labeled DNA. Drug−DNA mixtures were then incubated in the dark at room temperature for 17 h. Subsequently, digestion was initiated by adding 5 μL of 50 mM NaCl, 5 mM $MgCl_2$, and 5 mM $MnCl_2$ containing 0.02 units of DNase I to each well of the drug−DNA incubation plate. After 8 min the digestion was stopped by addition of 5 μL of 50 mM EDTA, and digested samples were purified, resuspended in 50 μL of 0.1 Tris-HCl, pH 8.5, concentrated to dryness, and resuspended in 0.8 μL of formamide containing 0.05% w/v bromophenol blue. Samples were denatured for 4 min at 95 °C and loaded onto a 48-lane sequencing gel (41 cm × 0.25 mm) containing 10 × TBE, 7 M urea, 10% formamide, and 5% Sequagel XR concentrate. Maxam−Gilbert G + A marker lanes were prepared accordingly. Gels were allowed to run for 6 h at 1500 V, 35 mA, 31.5 W, and 55 °C using a LI-COR model 4200 DNA sequencer with e-Seq, version 2.0 software (LI-COR Biosciences). The gel images were saved on the LI-COR equipment to allow visualization.

Gel Shift Assay. *Cell Lines and Culture Conditions.* NIH3T3 cells (obtained from the CRUK London Research Institute) were grown in Dulbecco's MEM high glucose (DMEM) (Autogen Bioclear) supplemented with 10% new-born calf serum (NBCS) and 1% glutamine, and incubated at 37 °C under 5% CO_2. HCT116 cells, obtained from the same source, were grown in RPMI medium (Bioclear) supplemented with 10% fetal calf serum (FCS) and 1% glutamine, and incubated at 37 °C under 5% CO_2.

Preparation of Nuclear Extracts. Nuclear extracts were prepared as previously described,[30] and all steps were performed at 4 °C in the presence of a protease inhibitor mix (Complete, Boehringer). Cells were rinsed with ice-cold phosphate buffered saline (PBS), scraped from the surface, and collected by centrifugation. They were then washed with 5 equivolumes of hypotonic buffer containing 10 mM K-Hepes, pH 7.9, 1.5 mM $MgCl_2$, 10 mM KCl, and 0.5 mM dithiothreitol (DTT, Sigma). Subsequently, the cells were resuspended in 3 equivolumes of hypotonic buffer, incubated on ice for 10 min, and subjected to 20 strokes of a Dounce homogenizer, and the nuclei collected by centrifugation. The nuclear pellet was resuspended in 0.5 equivolumes of low salt buffer containing 20 mM K-Hepes, pH 7.9, 0.2 mM K-EDTA, 25% glycerol, 1.5 mM $MgCl_2$, 20 mM KCl, and 0.5 mM DTT. While the mixture was stirred, 0.5 equivolume high salt buffer (as low salt buffer but containing 1.4 M KCl) was added, and the nuclei extracted for 30 min. The mixture was then centrifuged for 30 min at 14 000 rpm in an Eppendorf centrifuge, and the supernatant was dialyzed in tubing with a 12 kDa cutoff (Sigma) for 1 h in a 100-fold excess of dialysis buffer containing 20 mM K-Hepes, pH 7.9, 0.2 mM K-EDTA, 20% glycerol, 100 mM KCl, and 0.5 mM DTT. The dialyzed fraction was centrifuged for 30 min at 14 000 rpm in an Eppendorf centrifuge and the supernatant snap frozen in an ethanol−dry ice bath and stored at −80 °C. The protein concentration of the nuclear extract was assayed using a BIO-RAD microprotein assay kit.

Electrophoretic Mobility Shift Assay (EMSA). The oligonucleotides (MWG Biotech) containing ICB sites (underlined) used in the study were:

Topo IIα ICB1 sense, 5′-CGAGTCAGGG<u>ATTGG</u>CTGG-TCTGCTTC;
antisense, 5′-GAAGCAGACCAG<u>CCAAT</u>CCCTGACTCG;
Topo IIα ICB2 sense, 5′-GGCAAGCTACG<u>ATTGG</u>TT-CTTCTGGACG;
antisense, 5′-CGTCCAGAAGAA<u>CCAAT</u>CGTAGCTTGCC.

Oligonucleotides containing mutated ICBs were used as specific competitors of similar sequence, with the wild-type ICB sequence replaced with AAACC or GGTTT in sense and antisense oligonucleotides, respectively. Sense and antisense oligonucleotides were annealed in an equimolar ratio. Double-stranded oligonucleotides were 5′-end labeled with T4 kinase (NEB) using γ-^{32}P-ATP and subsequently purified on Bio-Gel P-6 columns (BIO-RAD). EMSAs were performed by incubating 10 μL of 5 μg nuclear extract at 4 °C for 30 min in a buffer containing 20 mM K-Hepes, pH 7.9, 1 mM $MgCl_2$, 0.5 mM K-EDTA, 10% glycerol, 50 mM KCl, 0.5 mM DTT, 0.5 μg poly(dI-dC)·poly(dI-dC) (Pharmacia), and 1× protease inhibitor mix (Complete, Boehringer). For supershifts, antibodies against NF-YA (IgG fraction, Rocklands) were used, and the preincubation on ice was extended for a total of 1.5 h. Upon addition of approximately 0.1 ng of radiolabeled probe, the incubation was continued for 2 h at room temperature. In competition experiments, radiolabeled probe and competitor were added simultaneously. Subsequently, 0.5 μL of loading buffer (25 mM Tris-Cl, pH 7.5, 0.02% BFB, and 10% glycerol) was added, and the samples were separated on a 4% polyacrylamide gel in 0.5 × TBE containing 2.5% glycerol at 4 °C. After the gels were dried, the radioactive signal was visualized by exposing the gels to Kodak X-Omat-LS film.

Molecular Modeling. Initial structures of the free ligands **1c**, **3a** and **3k** were made using the Schrodinger Maestro software,[35] with an approximate conformation established against the B-form DNA double helix being examined. Partial atomic charges were then assigned to the ligand using the Am1bcc charge strategy by means of the AMBER[36] antechamber software, with missing parameters assigned using parmchk. Standard B-form 15-mer DNA duplexes were constructed with the AMBER *nab* software. Xleap was then used to establish an initial graphical alignment of **3a** in the minor groove and to establish the initial coordinate and topology files using ff99bsc0 nucleic acid force field parameters and gaff parameters for the ligand. Prior to this step, 28 Na^+ counterions were automatically positioned, and a 10 Å truncated octahedral periodic water solvent box (TIP3P) was created for use in simulations along with periodic boundary conditions. Molecular dynamics simulations were run using PMEMD with a 2 fs time step, with SHAKE applied to all bonds to hydrogen atoms. Initial minimization of the water was carried out while restraining the DNA and ligand with a high force constant, followed by relaxation of the whole system without restraints. Dynamics (PMEMD) heating, with a periodic boundary from 0 to 300 K was then applied over 30 ps at

dx.doi.org/10.1021/jm4001852 | J. Med. Chem. XXXX, XXX, XXX−XXX

constant volume with the Langevin thermostat in operation (collision frequency of 1.0 ps^{-1}), and restraints applied to the DNA and ligand. Further equilibration at 300 K was then applied over 100 ps at constant pressure with no restraints in place. The final dynamics production run was carried out at constant volume at 300 K (NVT) over 10 ns. Throughout dynamic simulations, a time step of 2 fs was used, with the SHAKE algorithm applied to bonds involving H-atoms. AMBER, Version 11, and AmberTools, Version 1.5, were used, simulations being carried out with a single NVIDIA GPU card (GTX560 2Gb RAM). Dynamics were visualized with VMD[37] software. The same procedure was adopted for simulations involving the covalently bound ligand except that a covalent bond was established between the C11-position of **3a** and the C2-NH_2 of the appropriate guanine residue.

Free energy calculations were performed using the AMBER MM-PBSA approach, with constructs generated from the explicit solvent simulations (solvent removed). Of the 5000 frames saved during the 10 ns dynamics, 100 equally spaced frames were used for the free energy calculations. The average free energy was calculated from the set of frames.

Conformational variability over the course of the simulation was measured by comparing the coordinates of each frame (2 ps intervals) with the first frame, finding the best rms fit in each case.

■ ASSOCIATED CONTENT

Supporting Information

Synthesis of polyamide dimers (**6a−g**) and trimers (**8a−n**); synthesis of protected conjugates **10a−n**; analytical data for **1c**; NCI screening protocol; NCI screening results for **3a**; models of **3a** bound to DNA (Figures S1 and S2); plots of DNA groove width (Figures S3−S14). This material is available free of charge via the Internet at http://pubs.acs.org.

■ AUTHOR INFORMATION

Corresponding Author

*Telephone: +44 (0)7976 801535. E-mail: david.thurston@kcl.ac.uk.

Notes

JAH, PWH and DET have a financial interest in Spirogen Ltd.

■ ACKNOWLEDGMENTS

Cancer Research UK (CRUK) is thanked for financial support for part of this work (C180/A1060 to DET), and the EPSRC for an Earmarked QUOTA Studentship Award (01300211 to RMH). The NCI is gratefully acknowledged for providing the data from their 60 cell line screen.

■ REFERENCES

(1) Hsieh, M.-C.; Hu, W.-P.; Yu, H.-S.; Wu, W.-C.; Chang, L.-S.; Kao, Y.-H.; Wang, J.-J. A DC-81-indole conjugate agent suppresses melanoma A375 cell migration partially via interrupting VEGF production and stromal cell-derived factor-1alpha-mediated signaling. *Toxicol. Appl. Pharmacol.* **2011**, *255* (2), 150−159.

(2) Brucoli, F.; Hawkins, R. M.; James, C. H.; Wells, G.; Jenkins, T. C.; Ellis, T.; Hartley, J. A.; Howard, P. W.; Thurston, D. E. Novel C8-linked pyrrolobenzodiazepine (PBD)-heterocycle conjugates that recognize DNA sequences containing an inverted CCAAT box. *Bioorg. Med. Chem. Lett.* **2011**, *21* (12), 3780−3783.

(3) Hu, W.-P.; Tsai, F.-Y.; Yu, H.-S.; Sung, P.-J.; Chang, L.-S.; Wang, J.-J. Induction of apoptosis by DC-81-indole conjugate agent through NF-κB and JNK/AP-1 pathway. *Chem. Res. Toxicol.* **2008**, *21* (7), 1330−1336.

(4) Kotecha, M.; Kluza, J.; Wells, G.; O'Hare, C. C.; Forni, C.; Mantovani, R.; Howard, P. W.; Morris, P.; Thurston, D. E.; Hartley, J. A.; Hochhauser, D. Inhibition of DNA binding of the NF-Y transcription factor by the pyrrolobenzodiazepine-polyamide conjugate GWL-78. *Mol. Cancer Ther.* **2008**, *7* (5), 1319−1328.

(5) Berg, T. Inhibition of transcription factors with small organic molecules. *Curr. Opin. Chem. Biol.* **2008**, *12* (4), 464−471.

(6) Koehler, A. N. A complex task? Direct modulation of transcription factors with small molecules. *Curr. Opin. Chem. Biol.* **2010**, *14* (3), 331−340.

(7) Rahman, K. M.; Jackson, P. J. M.; James, C. H.; Basu, B. P.; Hartley, J. A.; De la Fuente, M.; Schatzlein, A.; Robson, M.; Pedley, R. B.; Pepper, C.; Fox, K. R.; Howard, P. W.; Thurston, D. E. GC-targeted C8-linked pyrrolobenzodiazepine-biaryl conjugates with femtomolar in vitro cytotoxicity and in vivo antitumor activity in mouse models. *J. Med. Chem.* **2013**, *56* (7), 2911−2935.

(8) Baraldi, P. G.; Cacciari, B.; Guiotto, A.; Romagnoli, R.; Spalluto, G.; Leoni, A.; Bianchi, N.; Feriotto, G.; Rutigliano, C.; Mischiati, C.; Gambari, R. Pyrrolo[2,1-*c*][1,4]benzodiazepine (PBD)-distamycin hybrid inhibits DNA binding to transcription factor Sp1. *Nucleosides, Nucleotides Nucleic Acids* **2000**, *19* (8), 1219−1229.

(9) Jansa, P.; Hatina, J. The inverted CCAAT motif is an indispensable element of the enhancer B of the mouse major histocompatibility class IH2-K-b gene. *DNA Cell Biol.* **2003**, *22* (1), 55−64.

(10) Ronchi, A.; Bellorini, M.; Mongelli, N.; Mantovani, R. CCAAT-box binding protein NF-Y (CBF, CP1) recognizes the minor groove and distorts DNA. *Nucleic Acids Res.* **1995**, *23*, 4565−4572.

(11) Marziali, G.; Perrotti, E.; Ilari, R.; Coccia, E. M.; Mantovani, R.; Testa, U.; Battistini, A. The activity of the CCAAT-box binding factor NF-Y is modulated through the regulated expression of its A subunit during monocyte to macrophage differentiation: regulation of tissue-specific genes through a ubiquitous transcription factor. *Blood* **1999**, *93* (2), 519−526.

(12) Hu, Q. H.; Maity, S. N. Stable expression of a dominant negative mutant of CCAAT binding factor/NF-Y in mouse fibroblast cells resulting in retardation of cell growth and inhibition of transcription of various cellular genes. *J. Biol. Chem.* **2000**, *275* (6), 4435−4444.

(13) Sullivan, D. M.; Latham, M. D.; Ross, W. E. Proliferation-dependent topoisomerase II content as a determinant of antineoplastic drug action in human, mouse, and Chinese hamster ovary cells. *Cancer Res.* **1987**, *47*, 3973−3979.

(14) Sandri, M. I.; Isaacs, R. J.; Ongkeko, W. M.; Harris, A. L.; Hickson, I. D.; Broggini, M.; Vikhanskaya, F. p53 regulates the minimal promoter of the human topoisomerase IIα gene. *Nucleic Acids Res.* **1996**, *24* (22), 4464−4470.

(15) Furukawa, M.; Ukiumi, T.; Nomoto, M.; Takano, H.; Morimoto, R. I.; Naito, S.; Kuwano, M.; Kohno, K. The role of an inverted CCAAT element in transcriptional activation of the human DNA topoisomerase IIα gene by heat shock. *J. Biol. Chem.* **1998**, *273* (17), 10550−10555.

(16) Isaacs, R. J.; Harris, A. L.; Hickson, I. D. Regulation of the human topoisomerase IIα gene promoter in confluence-arrested cells. *J. Biol. Chem.* **1996**, *271* (28), 16741−16747.

(17) Le, N. M.; Sielaff, A. M.; Cooper, A. J.; Mackay, H.; Brown, T.; Kotecha, M.; O'Hare, C.; Hochhauser, D.; Lee, M.; Hartley, J. A. Binding of f-PIP, a pyrrole- and imidazole-containing triamide to the inverted CCAAT box-2 of the topoisomerase II alpha promoter and modulation of gene expression in cells. *Bioorg. Med. Chem. Lett.* **2006**, *16* (24), 6161−6164.

(18) Hochhauser, D.; Kotecha, M.; O'Hare, C.; Morris, P. J.; Hartley, J. M.; Taherbhai, Z.; Harris, D.; Forni, C.; Mantovani, R.; Lee, M.; Hartley, J. A. Modulation of topoisomerase II alpha expression by a DNA sequence-specific polyamide. *Mol. Cancer Ther.* **2007**, *6* (1), 346−354.

(19) Mackay, H.; Brown, T.; Sexton, J. S.; Kotecha, M.; Nguyen, B.; Wilson, W. D.; Kluza, J.; Savic, B.; O'Hare, C.; Hochhauser, D.; Lee, M.; Hartley, J. A. Targeting the inverted CCAAT box-2 of the topoisomerase II alpha gene: DNA sequence selective recognition by a polyamide-intercalator as a staggered dimer. *Bioorg. Med. Chem.* **2008**, *16* (4), 2093−2102.

(20) Wells, G.; Martin, C. R. H.; Howard, P. W.; Sands, Z. A.; Laughton, C. A.; Tiberghien, A.; Woo, C. K.; Masterson, L. A.; Stephenson, M. J.; Hartley, J. A.; Jenkins, T. C.; Shnyder, S. D.; Loadman, P. M.; Waring, M. J.; Thurston, D. E. Design, synthesis, and biophysical and biological evaluation of a series of pyrrolobenzodiazepine-poly(*N*-methylpyrrole) conjugates. *J. Med. Chem.* **2006**, *49* (18), 5442−5461.
(21) Dervan, P. B. Molecular recognition of DNA by small molecules. *Bioorg. Med. Chem.* **2001**, *9* (9), 2215−2235.
(22) Swalley, S. E.; Baird, E. E.; Dervan, P. B. Recognition of a 5′-(A,T)GGG(A,T)2-3′ sequence in the minor groove of DNA by an eight-ring hairpin polyamide. *J. Am. Chem. Soc.* **1996**, *118* (35), 8198−8206.
(23) Boger, D. L.; Fink, B. E.; Hedrick, M. P. Total synthesis of distamycin A and 2640 analogs: a solution-phase combinatorial approach to the discovery of new, bioactive DNA binding agents and development of a rapid, high-throughput screen for determining relative DNA binding affinity or DNA binding sequence selectivity. *J. Am. Chem. Soc.* **2000**, *122* (27), 6382−6394.
(24) Fukuyama, T. L.; Liu, G.; Linton, S. D.; Lin, S. C.; Nishino, H. Total synthesis of (+)-porothramycin B. *Tetrahedron Lett.* **1993**, *34*, 2577−2580.
(25) Thurston, D. E.; Bose, D. S.; Howard, P. W.; Jenkins, T. C.; Leoni, A.; Baraldi, P. G.; Guiotto, A.; Cacciari, B.; Kelland, L. R.; Foloppe, M.-P.; Rault, S. Effect of A-ring modifications on the DNA-binding behavior and cytotoxicity of pyrrolo[2,1-*c*][1,4]-benzodiazepines. *J. Med. Chem.* **1999**, *42* (11), 1951−1964.
(26) Bose, D. S. ; Thompson, A. S. ; Smellie, M.; Berardini, M. D.; Hartley, J. A.; Jenkins, T. C.; Neidle, S.; Thurston, D. E. Effect of linker length on DNA-binding affinity, cross-linking efficiency and cytotoxicity of C8-linked pyrrolobenzodiazepine dimers. *Chem. Commun.* **1992**, *20*, 1518−1520.
(27) Gregson, S. J.; Howard, P. W.; Hartley, J. A.; Brooks, N. A.; Adams, L. J.; Jenkins, T. C.; Kelland, L. R.; Thurston, D. E. Design, synthesis, and evaluation of a novel pyrrolobenzodiazepine DNA-interactive agent with highly efficient cross-linking ability and potent cytotoxicity. *J. Med. Chem.* **2001**, *44*, 737−748.
(28) Gregson, S. J.; Howard, P. W.; Gullick, D. R.; Hamaguchi, A.; Corcoran, K. E.; Brooks, N. A.; Hartley, J. A.; Jenkins, T. C.; Patel, S.; Guille, M. J.; Thurston, D. E. Linker length modulates DNA cross-linking reactivity and cytotoxic potency of C8/C8′ ether-linked C2-exo-unsaturated pyrrolo[2,1-*c*][1,4]benzodiazepine (PBD) dimers. *J. Med. Chem.* **2004**, *47* (5), 1161−1174.
(29) Ellis, T.; Evans, D. A.; Martin, C. R. H.; Hartley, J. A. A 96-well DNase I footprinting screen for drug-DNA interactions. *Nucleic Acids Res.* **2007**, *35* (12), e89.
(30) Firth, J. D.; Ebert, B. L.; Pugh, C. W.; Ratcliffe, P. J. Oxygen-regulated control elements in the phosphoglycerate kinase 1 and lactate dehydrogenase A genes: similarities with the erythropoietin 3′ enhancer. *Proc. Natl. Acad. Sci. U.S.A.* **1994**, *91*, 6496−6500.
(31) Adams, L. J.; Jenkins, T. C.; Banting, L.; Thurston, D. E. Molecular modelling of a sequence-specific DNA-binding agent based on the pyrrolo[2,1-*c*][1,4]benzodiazepines. *Pharm. Pharmacol. Commun.* **1999**, *5*, 555−560.
(32) Rettig, M.; Weingarth, M.; Langel, W.; Kamal, A.; Kumar, P. P.; Weisz, K. Solution structure of a covalently bound pyrrolo[2,1-*c*][1,4]benzodiazepine-benzimidazole hybrid to a 10mer DNA duplex. *Biochemistry* **2009**, *48* (51), 12223−12232.
(33) Jones, G. B.; Davey, C. L.; Jenkins, T. C.; Kamal, A.; Kneale, G. G.; Neidle, S.; Webster, G. D.; Thurston, D. E. The noncovalent interaction of pyrrolo[2,1-c][1,4]benzodiazepine-5,11-diones with DNA. *Anti-Cancer Drug Des.* **1990**, *5* (3), 249−264.
(34) McConnaughie, A. W.; Jenkins, T. C. Novel acridine-triazenes as prototype combilexins: synthesis, DNA binding, and biological activity. *J. Med. Chem.* **1995**, *38* (18), 3488−3501.
(35) *Maestro*, version 9.2; Schrödinger, LLC: New York, NY, 2011.
(36) Case, D. A.; Darden, T. A.; Cheatham, T. E., III; Simmerling, C. L.; Wang, J.; Duke, R. E.; Luo, R.; Merz, K. M.; Pearlman, D. A.; Crowley, M.; Walker, R. C.; Zhang, W.; Wang, B.; Hayik, S.; Roitberg, A.; Seabra, G.; Wong, K. F.; Paesani, F.; Wu, X.; Brozell, S.; Tsui, V.; Gohlke, H.; Yang, L.; Tan, C.; Mongan, J.; Hornak, V.; Cui, G.; Beroza, P.; Mathews, D. H.; Schafmeister, C.; Ross, W. S.; Kollman, P. A. *AMBER*, version 9; University of California at San Francisco: San Francisco, CA, 2006.
(37) Humphrey, W.; Dalke, A.; Schulten, K. VMD: visual molecular dynamics. *J. Mol. Graphics* **1996**, *14* (1), 33−38.